ABSTRACT

Title of Thesis: VEHICLE PATH OPTIMIZATION OF
EMERGENCY LANE CHANGE MANEUVERS
FOR VEHICLE SIMULATION

Steven Robert O'Hara, Master of Science, 2005

Thesis directed by: Dr. Gregory A. Schultz
Department of Mechanical Engineering

Driver-based handling tests, such as the Double Lane Change (DLC) maneuver are subjective in nature and depend largely on driver skill and road conditions. They also suffer from poor repeatability. Implementation of these tests on hardware-in-the-loop simulators can also produce subjective results if the steer profiles are not systematically generated. This research produced a vehicle path optimization model that generated optimal paths for handling tests based on minimizing the maximum curvature during the maneuver. This approach lessened the dynamics of the vehicle and increased the chances of successful test results at given speeds. Excel's Solver was used for the optimization. The model results were compared to field test and hardware-in-the-loop test results, showing potential for reductions in lateral acceleration and vehicle side-slip.

VEHICLE PATH OPTIMIZATION OF

EMERGENCY LANE CHANGE MANEUVERS

FOR VEHICLE SIMULATION

by

Steven Robert O'Hara

Thesis submitted to the Faculty of the Graduate School of the
University of Maryland, College Park in partial fulfillment
of the requirements for the degree of
Master of Science
2005

Advisory Committee:

> Dr. Gregory A. Schultz, Chairman/Advisor
> Professor William Levine
> Professor Shapour Azarm

DEDICATION

To my family for their loving encouragement and support in all of my

endeavors

ACKNOWLEDGEMENTS

TABLE OF CONTENTS

LIST OF TABLES

LIST OF FIGURES

Chapter 1

Introduction

Vehicle safety has been a concern since the invention of the automobile. In 2002, 35.9% of all utility vehicle rollovers resulted in fatalities and a total of 11,217 Americans were fatally injured in rollover accidents. This accounts for 20.6% of all vehicular fatalities [4]. Consumer demand has shifted from the station wagon of years past to minivans and sport utility vehicles (SUVs). Such vehicles provide greater visibility, a larger hauling capacity and improved winter weather handling over sedans. However, SUVs have a higher center of gravity (cg) and are usually heavier than sedans, lessening the stability of the vehicle in high-speed cornering maneuvers.

Dynamic stability and directional response characteristics are important factors in the safety of a vehicle. Dynamic stability is the measure of a vehicle's resistance to spin-out or tip-up while in motion, both of which contribute to rollover situations. Though dependent on the vehicle's cg height and suspension characteristics [2], dynamic stability is also largely affected by the driver's interaction with the vehicle.

A number of handling tests are used to determine the closed-loop dynamic stability of the vehicle. During the test the vehicle/driver pair is a closed-loop system,

where the driver is constantly evaluating the vehicle's response and controlling the appropriate steering and acceleration inputs to complete a desired maneuver. Conversely, directional response tests strictly measure the vehicle's open-loop response to a given steering input [12], independent of the driver. Handling tests that include the closed-loop pair produce subjective results in comparison to open-loop directional response tests. The subjective quality of handling tests also produce testing variability, which is greatly reduced in directional response maneuvers.

In November 2000, Congress enacted the Transportation Recall Enhancement, Accountability and Documentation (TREAD) Act. In Section 12 of the TREAD Act, the National Highway and Traffic Safety Administration (NHTSA) was directed to "develop a dynamic test on rollovers by motor vehicles for a consumer information program conducting such test." This dynamic rollover resistance rating test will be incorporated into NHTSA's New Car Assessment Program (NCAP)[9]. In Phases IV, V and VI of NHTSA's light vehicle dynamic rollover research program presentation [7], various handling maneuvers were discussed. These maneuvers were broken into three types: automated steering, driver-based steering, and computer-corrected driver-based steering.

The automated steering maneuvers consisted of the NHTSA J-Turn, Fixed Timing Fishhook, Roll Rate Feedback Fishhook, Nissan Fishhook and the Open-Loop Pseudo-Double Lane Change, and were designed to test the directional response of the vehicle. However, these maneuvers were criticized as being an unrealistic representation of true emergency maneuvers [9]. The Open-Loop Pseudo-Double Lane Change maneuver was based on actual driver data, thus resulting in some level of realistic driver interaction.

The driver-based steering tests consisted of the International Organization for

Standardization (ISO) 3888 Part 2 and the Consumers Union (CU) Short Course, in addition to the computer-corrected Ford PCL LC maneuver. The driver-based maneuvers, which are all double lane change (DLC) maneuvers, are realistic in nature but create varying results depending on the driver's skill and responses. The U.S. military also uses two DLC maneuvers to assess heavy truck rollover propensity, these are named the NATO Test and TOP test. The NATO test is very similar in format to the ISO 3888 Part 2, and the TOP test is very similar in format to the CU Short Course test.

All of the open-loop and closed-loop steering maneuvers are typically conducted on test tracks with human drivers in the vehicles. Accordingly, a level of risk is associated with each test operation. During the open-loop tests, a robotically-controlled steering actuator executes the steering command. The driver temporarily relinquishes control of the vehicle during the maneuver and then reassumes control after the test event. This can be somewhat unnerving to test drivers. The other risk is that of potential yaw and roll instability. Outriggers, Figure 1.1, are generally outfitted on vehicles under open and closed-loop tests to prevent rollover from occurring. The inertia of the outriggers can affect the dynamics of the vehicle in the yaw and roll directions, and thus can affect the test results. Improvements to outrigger design have been made in an effort to decrease their weight and effect on the vehicles inertial response, but are very expensive. Use of outriggers during field tests are nonetheless essential when testing the limits of a vehicle's rollover resistance.

The U.S. Army Aberdeen Test Center has built the capability to perform handling tests of vehicles in a laboratory environment at their Roadway Simulator (RWS) facility, described later in this chapter. Two of the reasons for building the

3

Figure 1.1: Aluminum and Carbon Fiber Outriggers used by NHTSA [7]

RWS facility were to remove the driver from a relatively unsafe environment and to remove the requirement for outriggers. Open-loop steering tests are executed by a steering robot, while the closed-loop dynamics of the vehicle are simulated. Closed-loop and DLC maneuver tests are executed by iteratively conducting test trials using a series of "best guess" steering profiles. Similar to the use of drivers in the field tests, the results of DLC tests on the RWS are subjectively dependent on the test engineers skill in choosing the steering profiles.

Problem Definition Statement

The primary objective of this research was to improve repeatability and reduce subjectivity of DLC maneuver tests, thus improving the effectiveness of these tests. This was accomplished by systematically generating optimal paths for tests at different vehicle speeds that minimized system dynamics. An optimization computer model was created and used to minimize the maximum (or peak) curvature over double lane change maneuver tests, thus minimizing the affects of lateral acceleration on the vehicle. The path optimization model is applicable to the RWS and

field tests and may be generally useful for autonomous control of ground vehicles.

This thesis focuses on developing an optimal vehicle test path for the NATO DLC maneuver for use on a Roadway Simulator and other field tests. The NATO DLC was selected because of its rigorous requirements and dependence upon vehicle dimensions. The goal of the NATO DLC maneuver is to determine the greatest constant forward speed a vehicle is able to obtain without failing the requirements of the test. A test is failed when the vehicle experiences wheel tip-up, vehicle spin-out that causes the vehicle to exit the course, or power-limitation resulting in a drop in vehicle speed.

The path optimization model developed in this thesis is also applicable to the general problem of determining an optimal path through any series of course constraints that minimizes the maximum path curvature with the intent of minimizing the vehicle's dynamics during the maneuver.

1.1   The Double Lane Change Maneuver

There are six main forms of the DLC maneuver discussed in the literature. We will classify these into four main types of lane changes: standard, object-avoidance, path-corrected, and computer-generated. The ISO 3888 part 2 and the NATO Emergency Lane Change maneuver (Figure 1.2) are designated as a "standard" lane change. The objective of this type of DLC maneuver is for the vehicle to begin in one lane, enter a second lane and remain in that lane for a certain distance before returning to the original lane. Lane width is similar for both the ISO and NATO course, however, the distance between the various sections of NATO course are dependent upon vehicle length.

The second type of the DLC maneuver is designed to test object avoidance.

Both the CU short course and the TOP Emergency Lane Change maneuver (Figure 1.3) require the vehicle to exit the lane of origin to avoid a road obstruction and immediately return to the original lane. In testing each of these maneuvers, cones (pylons) are used to mark course limits.

The third type of DLC maneuver is the Ford Path-Corrected Limit (PCL) Lane Change (LC). Similar in format to the previous two types, this is a driver-based test. However, in this test, the driver runs three slightly different versions of a DLC maneuver. Ford Motor Company has developed a proprietary analysis technique that removes driver variation from the data, hence improving the ability to accurately compare vehicle test results. The fourth type of DLC maneuver develops a computer-generated steering command based on successful driver steering histories of the first two types of DLC maneuvers.
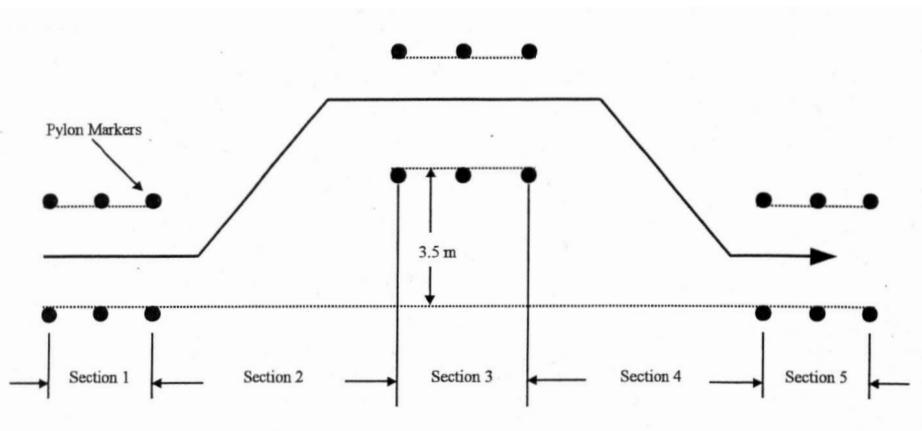
Figure 1.2: NATO Emergency Lane Change Course [27]

NHTSA conducted a detailed evaluation of four types of DLC maneuvers: the CU Short Course, the ISO 3888, the Ford PCL LC and the Open-Loop Pseudo DLC [9]. Each type of the maneuver was rated on a Likert scale from 'very bad' to 'excellent'. The summary of the results is presented in Table 1.1.

All forms of the DLC maneuver were found to accurately represent realistic emergency driving situations. With the exception of the Open-Loop Pseudo-DLC, each form of the maneuver required direct driver interaction. Based on this study, tests requiring human driver interaction have been shown to result in a poor repeatability factor for the overall test. However, The Open-Loop Pseudo DLC resulted in satisfactory repeatability due to consistent computer-generated steering commands based on driver steering histories. This shows that a significant degree of subjectivity is removed when the steering commands for the maneuver are computer-generated.

This research took the concept of the Open-Loop Pseudo DLC a step further. Rather than developing open-loop steer commands based on previous standard and object avoidance maneuvers, the focus of this research was on generating a path with minimized lateral acceleration using path optimization. This removed the requirement to conduct a series of DLC maneuvers, therefore reducing the amount of testing required.
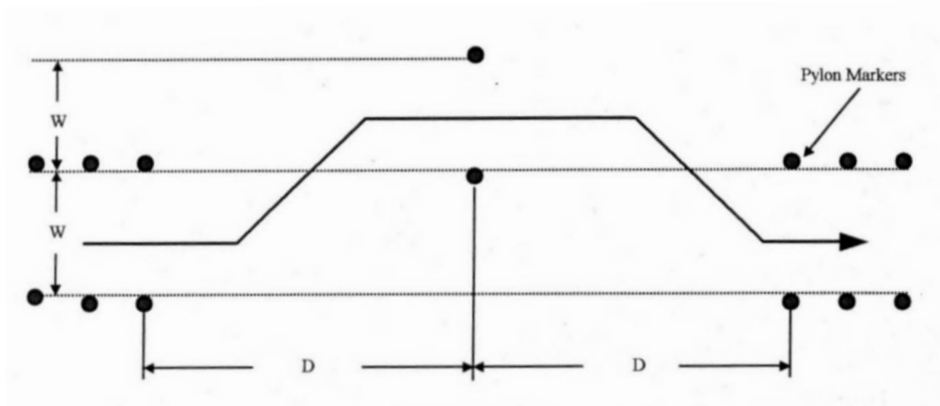
Figure 1.3: TOP Emergency Lane Change Course [27]

Table 1.1: NHTSA Rollover Resistance Maneuver Scores [9].

Assessment Criterion	CUSC	ISO 3888 Part 2	Ford PCL LC	Open-Loop Pseudo-Double Lane Change
Objectivity and Repeatability	Bad	Bad	Bad	Satisfactory
Performability	Satisfactory	Good	Satisfactory	Satisfactory
Discriminatory Capability	Very Bad	Very Bad	Good	Very Bad
Appearance of Reality	Excellent	Excellent	Excellent	Excellent

1.2 Vehicle Simulation

Vehicle simulation has reduced the time required to develop and test a vehicle, therefore reducing the vehicle's time to market. There are three stages which the automotive industry must perform in designing and introducing a vehicle [27]. The first stage is field testing, which requires evaluation of current vehicle designs and components to determine the proper improvements and implementations. The second stage, computer simulation, provides a means to evaluate a new design before it is manufactured. Current computer modelling is used to determine performance characteristics and failure analysis, as well as an overall view of the vehicle. The final stage of design involves physically testing the vehicle through rigorous courses and vehicle component tests. This process is used to test the vehicle's handling, response and reliability.

Automotive manufacturers have developed testing courses and proving grounds for the purpose of testing improvements to existing vehicles, new vehicles and new vehicle components. The use of vehicle simulation for these design stages greatly reduces the length of time required for the design process. Vehicle simulation allows for complete control of the testing environment because testing is independent of environmental conditions on the test course. Conditions such as rain, snow, ice, wind, heat and cold can be completely eliminated or specifically generated. Additionally, data acquisition is improved in the quantity of information received and its rapid collection time. Under current course testing practices, it is necessary to carry the majority of the testing instrumentation within the vehicle. Harsh testing conditions can cause sensitive instrumentation to fail consequently producing inaccurate information about the vehicle's operating conditions. However, in simulation testing, the main data collection equipment can be located external to the vehicle, bridged by wires or through a wireless network interface.

There are three major types of vehicle simulation: software-in-the-loop, driver-in-the-loop and hardware-in-the-loop. The advantage of software-in-the-loop modelling is the ability to test a design before it is produced. The dynamics of the vehicle are modelled and simulated within a vehicle program, based on the characteristics of the vehicle being studied. This method is extremely cost-effective and useful in determining the general behavior and characteristics of a design. However, the accuracy of the results generated from complete computer models is greatly dependent upon the type of model and supporting data.

Driver-in-the-loop simulators retrieve valuable information related to human driving characteristics. The National Advanced Driver Simulator (NADS) [26] is an example of this type of simulator, in which the driver is placed in a mock vehicle

cab containing controls and a computer-generated view of the roadview picture. This type of simulation replicates the response inertial forces created from various maneuvers generated by the driver and is generally intended for human factor testing.

Hardware-in-the-loop removes the difficulties and errors intrinsic in creating a computer-based vehicle model, emphasizing the input commands and output results of the vehicle. Information received from driver-in-the-loop simulators aids in the creation of driver models used to run such hardware-in-the-loop simulators. A great value of hardware-in-the-loop testing is the elimination of driver interaction and subjectivity by directly testing the vehicle (hardware) of interest. Testing the hardware directly eliminates the need for a mathematical model of the vehicle, which could introduce errors to the test. MTS created a Roadway Simulator (RWS) for use at the U.S. Army Aberdeen Test Center (ATC). The Roadway Simulator allows a vehicle to be tested in its entirety while being operated in a simulated road environment. This simulator functions as a hardware-in-the-loop simulator and will be used to implement the research developed within this thesis.

1.2.1   The Roadway Simulator

The RWS (Figure 1.4) consists of four flat-trac units. Each unit utilizes a seamless stainless steel belt resting on top of a flat water-bearing platform. This platform is located between the two end drums of the unit. Two main restraint arms are responsible for maintaining the vehicle's position on top of the four flat-trac units. The restraints contain bi-axial load-cells, used to measure the forces generated by the vehicle in the constrained directions. These restraints can either be positioned on the sides of the vehicle or front and rear through its center of mass or roll axis.

ATC Roadway Corner - Pictorial
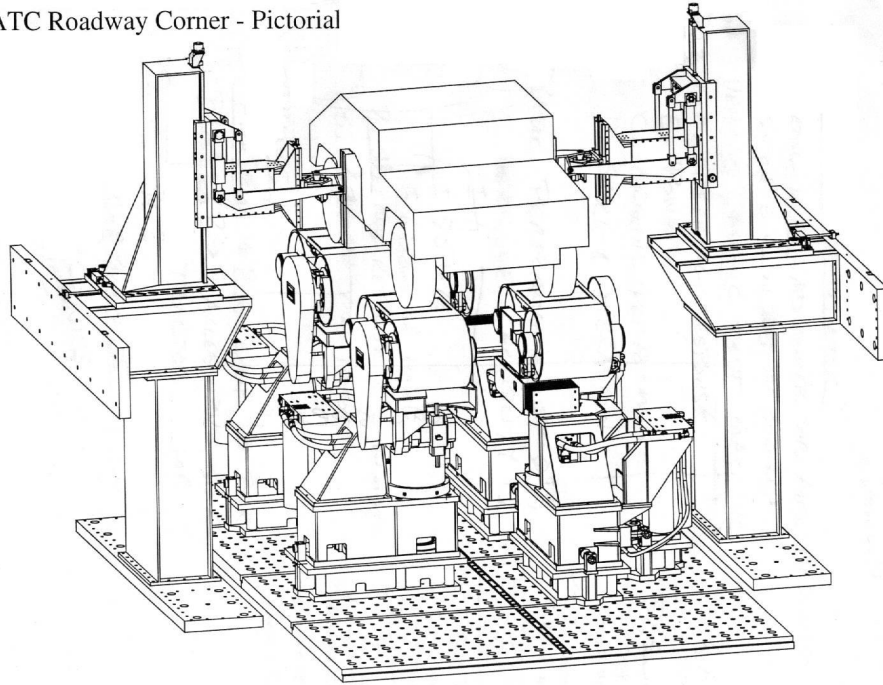
Figure 1.4: The U.S. Army Aberdeen Test Center's Roadway Simulator (RWS) [27]

The vehicle is adaptively constrained upon the RWS such that there are three constrained degrees of freedom and three free degrees of freedom. The vehicle is constrained in the x-axis, y-axis and yaw directions. However, the vehicle is able to move in pitch, roll and the z-axis directions. The load-cells on the two restraint arms are used to compute the vehicle's longitudinal (u), lateral (v) and yaw (r) velocities, using D'Alembert's Principle. Figure 1.5 shows the associated standard Society of Automotive (SAE) sign convention. The simulation basic period is one millisecond. The velocity values are used with the vehicle wheelbase (L), track width (t), and center of gravity location data to determine necessary steer angles and road speeds for each of the four flat-trac units. The flat-trac directional

response times are on the order of 0.010 to 0.025 seconds, depending on the settings of the controller gain values. These times are considerably faster than the steering response of typical passenger vehicles, which have a practical bandwidth of 1 to 2 Hz.
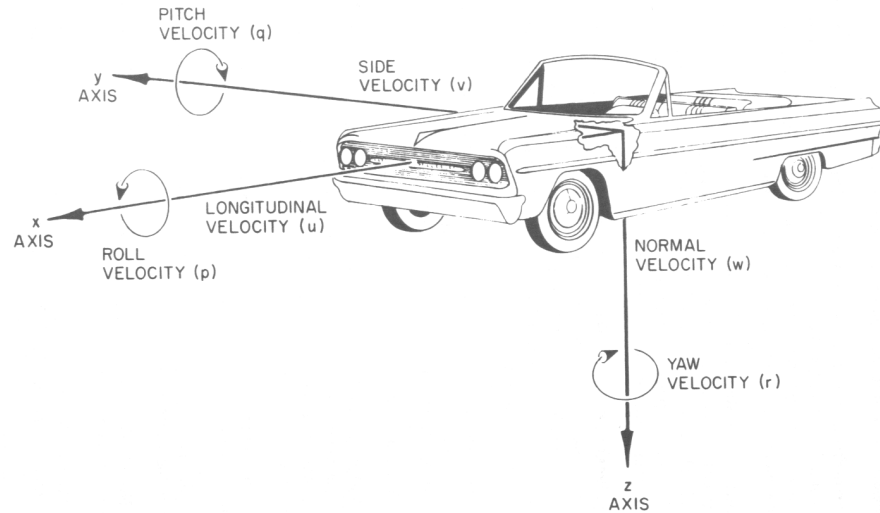
Figure 1.5: Standard Society of Automotive Engineers (SAE) Sign Convention [12]

The RWS provides a robotic driver with steering, braking, throttle and shifting capability. Control can be either closed-loop or open-loop depending on the test. For the NATO DLC maneuver test the throttle is controlled to maintain constant vehicle path speed while an open-loop steer command profile is executed by the steer actuator. For constant-radius skid pad tests closed-loop control of the steer actuator is used to maintain constant curvature.

Currently , DLC testing on the RWS is conducted iteratively in a time-intensive manner. The test operator estimates an appropriate open-loop steer profile for a relatively low vehicle speed based on experience and previous test results. The operator executes the tests and adjusts steer points until the vehicle negotiates

the course without hitting the course boundaries. The test speed is increased in small steps with constant revision to the steer profile until a speed is reached that the vehicle can no longer negotiate the course without going unstable or crossing course boundaries. As mentioned earlier this approach is still rather subjective in nature. Experience has shown that the top vehicle speeds observed on the RWS are slightly higher than in the field, most likely because the RWS operator and steer robot can operate without fear of injury. Accordingly, a more unified, systematic and consistent approach is required to generate the open-loop DLC steer profiles.

1.3 Literature Review

1.3.1 Rollover Testing and Dynamic Response

NHTSA has produced a thorough evaluation of various emergency response maneuvers in an attempt to determine the best way to evaluate a vehicle's stability response. Specific work focusing on the category of Double Lane Change maneuvers is evaluated in [9]. NHTSA also examined the J-turn and Fishhook maneuvers in [8]. The focus of these studies was untripped vehicle rollover with the intent of eliminating external rollover factors. A detailed report of NHTSA's rollover test evaluation work applied to 26 different vehicles is discussed in [10]. Additionally, NHTSA presented its goals in achieving the objectives of the TREAD act; the various phases involved in light vehicle rollover testing are discussed in [7].

Rollover research is of great interest because of the ever-present need to improve vehicle safety. Computer simulation was conducted by [22] and [2] to determine the characteristics of vehicle handling and stability in an emergency object avoidance maneuver. Marine accurately discussed two primary rollover scenarios in [20].

The first was loss of directional control, where a large vehicle side-slip angle (β) was developed. The second scenario was an excitation of the vehicle's roll mode through an increased roll angle (ϕ). These are discussed further in Chapter Two. Simulation software was used by Frimberger in [11] for the purpose of modelling tripped vehicle rollover.

1.3.2 Simulation

It was previously discussed that vehicle simulation is useful in a variety of contexts. DaimlerChrysler has conducted very extensive research based on the application of software-in-the-loop, rapid prototyping and hardware-in-the-loop testing [30]. Its interest as a car manufacturer is a reduced production cost and a reduction in the time required to test parts or a vehicle's configuration. Simulation is also useful in modelling driver-vehicle interaction. A very simple hardware-in-the-loop simulator was utilized in [25] to develop the parameters of a driver model while conducting DLC testing. Allen conducted extensive development of a software model named VDANL used to test vehicle dynamic response [2] and driver-vehicle modelling [1]. A thorough discussion of various driver-in-the-loop simulators is presented in [13]. Additional discussion of the NADS Simulator is presented in [26].

Other mathematical simulation approaches have been proposed. "Force-Moment analysis was first presented in a 1952 Cornell Aeronautical Laboratory (CAL) memo titled, 'Long Range Stability and Control Research Program' by Bill Milliken [21]." The fundamentals of the Force-Moment method are discussed in the Milliken Research Associates (MRA) Moment Method. The first development of MMM computer programs began in 1976 by General Motors [21]. The method is based on intensive steady-state cornering test data. However, the approach is

often considered impractical and may not accurately account for dynamic events.

The current state-of-the-art in hardware-in-the-loop simulation is the product of over three decades of research and development. The first patent for a roadway simulator was submitted by General Motors on November 8, 1967 and granted on July 14, 1970 as US patent 3,520,180 [23]. Early designs resembled vehicle dynamometers, machines used to measure the torque and horsepower a vehicle is able to create. Certain designs were as simplistic as placing a vehicle on a moving belt and tying down the vehicle while the belt moved beneath it. However, these designs failed to account for wheel slip in the steer directions, and thus prevented early simulators from conducting corner tests. The absence of a flat ground plane on early simulators also resulted in errors in tire forces.

In 1995 Langer from MTS Systems Corporation introduced the first flat-surface Roadway Simulator [17, 18]. Two machines were installed at Fiat's facility in Italy in 1997, and were sized for passenger cars up to 5000 pounds gross vehicle weight (GVW) [28]. In 2003, the U.S. Army Aberdeen Test Center opened the Roadway Simulator test facility, sized primarily for trucks over 5000 pounds GVW. All three machines were essentially the same basic design. The advantage of this new generation of hardware-in-the-loop simulator was the ability to conduct cornering test with flat ground planes. ATC introduced improvements in dynamics calculations and controller implementation to MTS's simulator.

1.3.3 Path Optimization

A driver directional control model was developed by Guan in [14] and [15], utilizing a fuzzy decision making model to simulate a vehicle driver. The model used a course look-ahead distance to simulate a fixed preview distance available to the

driver. However, the focus of the fuzzy model was to replicate driver decision-making for course maneuvering. The chance of obtaining a successful test path using this model is dependent upon the model's representation of the driver. Though this approach created a repeatable path for imitating driver interaction, the results of Guan's model are not applicable to this research, which focused on vehicle response.

Vehicle path optimization was also tested by Prokop [24] in conjunction with vehicle driver modelling. Prokop's optimization objectives were to minimize: time, acceleration, brake effort, steering, engine rpm and velocity. The impetus was to further understand human driving motives and model those preferences. Prokop effectively demonstrated that the determination of an optimal path was dependent upon the optimization objective. However, the results were again highly dependent upon the driver model.

Bernard utilized Genetic Algorithms to determine the best course for a vehicle through the Consumers Union Short Course test [3]. This produced effective results and provided a framework with little dependence upon a driver model. The model accounted for the vehicle dynamics, vehicle state and potentially driver interaction. The convergence toward an appropriate test path was dependent upon the fitness function of the model, and the evolution to the final result. Though this model was shown to be robust, repeatability across multiple vehicle platforms was dependent upon the modelling of each vehicle.

A steering robot has also been tested and validated by Tseng et al. [29] for the purpose of steering a vehicle through a predetermined path. The results showed effective maneuvering of a double lane change test. However, Tseng did not describe how the path was formed.

16

Fraichard presented an effective study of constant curvature path optimization for car-like robotic vehicles [6]. This article discussed bounded curvature and bounded rate of change of curvature optimization in path generation. This work provided a solution to the curvature step change present in strictly constant curvature optimization paths. However, the clothoid arcs used to generate a constant rate of change of curvature increased the overall curvature of the path. The model presented did not account for the dynamics and side-slip of the robotic vehicle. Nonetheless, this work provided an interesting parallel to the constant curvature path optimization model presented in this thesis.

The research presented in this thesis developed an optimal path generation model dependent upon vehicle characteristics and test speed. This new model is independent of driver-modelling and focuses on optimization of vehicle stability by minimizing system dynamics.

1.4   Thesis Organization

Chapter Two focuses on vehicle dynamics and discusses the specific handling characteristics that affect a test vehicle's ability to maneuver a course. This provides the basis for choosing the optimal path as the one that produces the lowest peak path curvature. The idea is that minimizing the lateral acceleration of a cornering maneuver minimizes the dynamics of a vehicle, thus providing the best conditions and chances for success.

In Chapter Three, an optimization model is developed using Microsoft Excel's Solver. The model was used to generate an optimal vehicle trajectory for a given vehicle course. The model used the NATO DLC course layout to demonstrate vehicle path generation given a constrained course. The path optimization model

also provided evidence that the optimal path consisted of continuous segments of constant curvature.

Chapter Four compares vehicle paths and characteristics produced by the path optimization model with data collected on the RWS and in field testing. This was used to validate the ability of the model to develop a realistic path in comparison to current test data. Chapter Five concludes with an overall summary of the work presented and areas of future work and development.

Chapter 2

Vehicle Dynamics and Path Optimization

2.1   Vehicle Dynamics

This chapter discusses the basic dynamics of vehicle tip-up and spin-out. The goal is to provide justification for the creation of optimal paths for the DLC maneuver that minimize lateral acceleration. Throughout this paper and much of the rollover testing literature, the focus is on untripped vehicle rollover. Tripped vehicle rollover is the result of a vehicle hitting an obstruction such as a curb, an embankment, or a variation in the road surface.

Vehicle tip-up and spin-out signify that the vehicle's dynamic stability has become compromised, indicating a possible rollover if the unbalanced forces on the vehicle continue to increase. By understanding the dynamics leading up to rollover, we are able to effectively measure and assess the vehicle's stability using tests like the NATO DLC. First, it is necessary to explain vehicle tip-up mechanics under simulated static load conditions. Afterwards, some basic mechanics equations for cornering are discussed as they relate to vehicle roll and yaw motion versus lateral acceleration.

2.1.1 Static and Quasi-Static Vehicle Stability
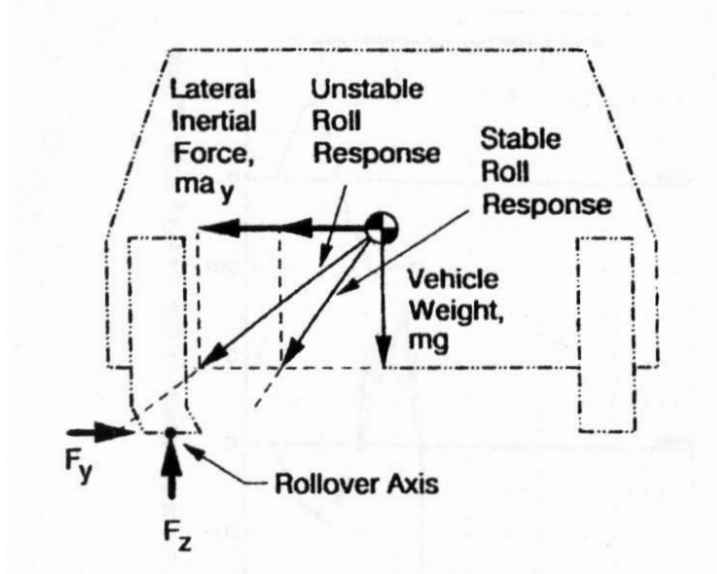
Figure 2.1: Stable and Unstable Llateral Forcing Affecting a Static Vehicle [2]

Static stability is a measure of a vehicle's propensity to tip-up under simulated lateral acceleration conditions when stationary. As a starting point, a basic calculation can be conducted where the fundamental forces and moments leading to vehicle rollover are summed to roughly estimate the vehicle's rollover threshold. These basic forces are illustrated by Allen in Figure 2.1. If the vehicle is on level ground, its rollover threshold becomes simply a function of the vehicle's track width (t) and cg height (h) as displayed in Equation (2.1). The rollover threshold represents the maximum lateral acceleration value that the vehicle is able to reach before tipping up. Increasing the vehicle's track width or reducing its cg height improves the rollover threshold of the vehicle. The rollover threshold is also referred to as the Static Stability Factor (SSF) in the literature.

$$\frac{a_y}{g} = \frac{t}{2h} \tag{2.1}$$

where

$$a_y \quad = \quad Lateral\ acceleration$$

$$g \quad = \quad Gravitational\ acceleration$$

$$t \quad = \quad Vehicle\ track\ width$$

$$h \quad = \quad Height\ of\ the\ vehicle's\ cg\ above\ the\ ground$$

The static stability analysis is helpful in producing a conservative rollover threshold estimate for the vehicle. Gillespie defines a quasi-static threshold which accounts for the body roll angle (φ) of the vehicle [12]. As the vehicle body (sprung mass) is able to roll with respect to the chassis (unsprung mass) the amount of lateral acceleration necessary to develop rollover is decreased, thus lowering the rollover threshold of the vehicle. In the static stability model, the roll axis is located at the contact point of the outer wheel. In the quasi-static model, the roll center of the vehicle is at the location of the kinematic roll axis. Gillespie defines the rollover threshold of a suspended vehicle with the following relationship.

$$\frac{a_y}{g} = \left[\frac{1}{1 + R_\phi (1 - \frac{h_r}{h})} \right] \frac{t}{2h} \tag{2.2}$$

where

$$h_r \quad = \quad Height\ of\ the\ vehicle's\ roll\ center\ above\ the\ ground\ at\ the\ cg\ location$$

$$R_\phi \quad = \quad Roll\ Rate\ (radians/g)$$

Neither the SSF or quasi-static estimates account for the tire deflection or chassis compliance. Increased precision is obtained using various static stability

tests conducted on tilt tables or with cable tether systems. While these provide improved estimates, they do not account for the true dynamics of the vehicle during a cornering maneuver.

2.1.2 Vehicle Cornering

The lateral acceleration of a vehicle (a_y) during cornering is given by Equation 2.3. This shows a direct relationship between the lateral acceleration and the curvature (ρ) of the path. The ability of a vehicle to achieve a given level of lateral acceleration is dependent on a number of nonlinear variables. These include the cornering stiffness of the front and rear tires, cg location, suspension kinematics, stiffness and compliance, and steering kinematics. In general terms, the steering angle (δ) of the front wheels and the lateral acceleration are related by Equation 2.4 under steady-state cornering conditions.

$$a_y = \frac{V^2}{R} = V^2 \rho \tag{2.3}$$

where

$$
\begin{aligned}
V &= \ Forward\ vehicle\ velocity\ along\ the\ path \\
R &= \ The\ radius\ of\ the\ path\ at\ the\ location\ of\ interest \\
\rho &= \ The\ curvature\ of\ the\ path\ at\ the\ location\ of\ interest
\end{aligned}
$$

$$\delta = \frac{L}{R} + K a_y \tag{2.4}$$

where

$$
\begin{aligned}
\frac{L}{R} &= \ Ackerman\ steer\ angle\ (radians)\ under\ low-speed\ cornering \\
K &= \ The\ understeer\ gradient
\end{aligned}
$$

The understeer gradient largely determines the steering behavior of a vehicle. If it is positive the vehicle will understeer the intended path, if it is negative it will over steer the intended path, and if it is zero it will result in a vehicle with neutral steering characteristics. A detailed discussion of the understeer gradient is beyond the scope of this paper, but is heavily influenced by tire weight transfer during vehicle roll. In some cases, reduced tire cornering forces due to excessive roll, low cornering stiffness, or high roll stiffness can relieve the lateral acceleration and reduce the risk of tip-up and rollover. However this is not always the case.
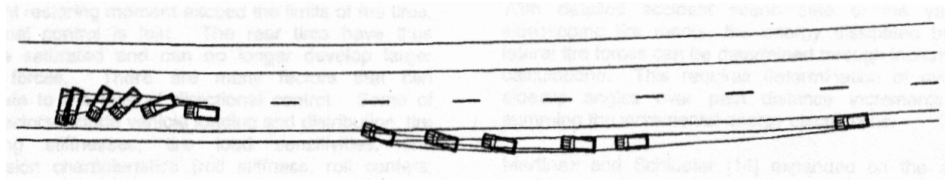
Figure 2.2: Two Scenarios Leading to Vehicle Rollover [20]

There are two primary handling behaviors related to vehicle stability. The first is loss of directional control, where a large body side-slip angle (β) is developed. This large side-slip angle leads to vehicle spin-out. The second scenario is an excitation of the vehicle's roll mode through an increased roll angle (ϕ). This will lead to vehicle tip-up and ultimately to rollover if the dynamic instabilities continue to increase. These two scenarios are shown in Figure 2.2 and discussed further by Marine in [20]. Loss of directional control can also lead to tip-up if the vehicle's orientation becomes such that it is nearly perpendicular to the velocity vector.

Dynamics Leading to Tip-Up

Vehicle tire tip-up was discussed as one of the three primary mechanisms that will end a DLC test. A vehicle's susceptibility to tip-up will increase as the lateral acceleration upon the vehicle increases. From Equation 2.3 we can conclude that limiting the curvature of the path will limit the effects leading to vehicle tip-up during steady-state and transient maneuvers. Roll angle (ϕ) and roll rate ($\dot{\phi}$) are also directly related to the lateral acceleration of the vehicle. Roll rate can be a significant factor during transient maneuvers since the roll inertia of the vehicle can add a substantial roll moment if the roll rate varies. Nonetheless, reducing lateral acceleration and rate of change of lateral acceleration will reduce the chances of tip-up.

Dynamics Leading to Spin-Out

Vehicle spin-out is a condition that is created when the vehicle's body side-slip angle (β) becomes too large. Beta is the angle between the vehicle's heading direction and the direction of travel. By manipulating Equation 6-23 in Gillespie [12], we obtain Equation 2.5, where an increase in the curvature or lateral acceleration also increases the body side-slip angle of the vehicle. Figure 2.3 illustrates a plot of vehicle body side-slip versus lateral acceleration obtained from a DLC test on the RWS. Using a polynomial fit, a close approximation can be developed to determine the vehicle's side-slip angle as a function of the vehicle's lateral acceleration for near steady-state conditions. Side-slip characterization during more transient conditions requires modelling of steering frequency response data, as will be discussed in Chapter Three.

$$\beta = \rho\left(c - \frac{w_r V^2}{c_{\alpha r} g}\right) = \left(c\rho - \frac{w_r}{c_{\alpha r}}\frac{v^2 \rho}{g}\right) = \left(c\rho - \frac{w_r}{c_{\alpha r}}\frac{a_y}{g}\right) \tag{2.5}$$

where

$$c \quad = \quad Distance\ between\ the\ cg\ and\ the\ rear\ axle$$

$$w_r \quad = \quad The\ load\ on\ the\ rear\ axle$$

$$c_{\alpha r} \quad = \quad The\ cornering\ stiffness\ of\ the\ rear\ tires$$
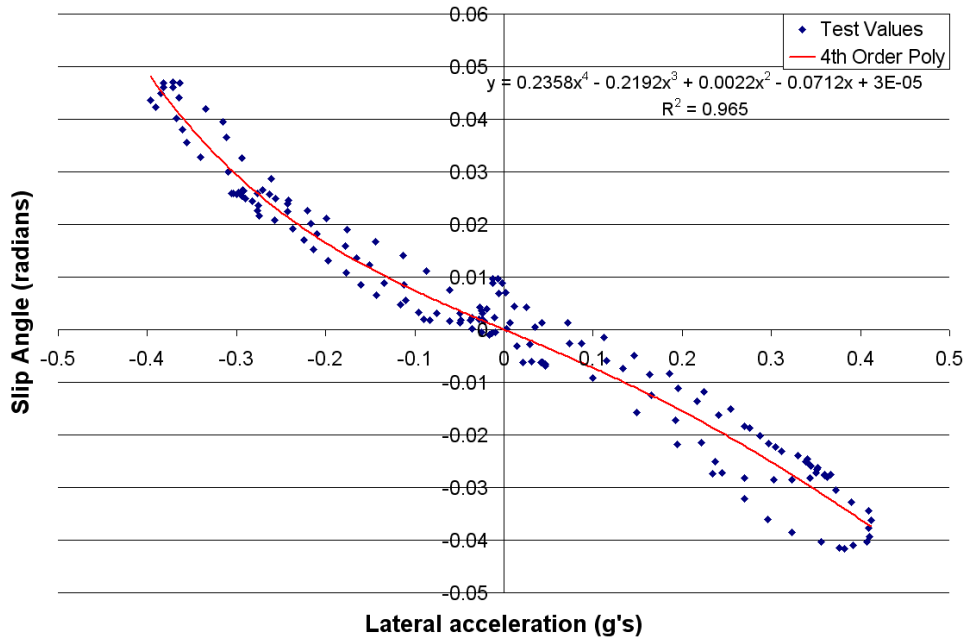
Figure 2.3: Vehicle Body Side-Slip Versus Lateral Acceleration

Directional stability is a very complicated subject and is influenced by many vehicle design choices and loading conditions. During a transient maneuver, the rate of change of vehicle's side-slip angle $(\dot{\beta})$ is a key indicator of vehicle stability. Therefore $\dot{\beta}$ or even yaw rate (r) must also be minimized to improve vehicle stability. A more precise statement of Equation 2.3 is given by,

$$a_y = \dot{v} + ur \tag{2.6}$$

where

$$
\begin{aligned}
u &= \ \textit{Longitudinal velocity} \\
v &= \ \textit{Lateral velocity} \\
r &= \ \textit{Yaw velocity}
\end{aligned}
$$

Assuming $u = V = $ constant forward velocity, we obtain:

$$a_y = \dot{v} + Vr \tag{2.7}$$

By definition

$$\beta = tan^{-1}\left(\frac{v}{u}\right) = tan^{-1}\left(\frac{v}{V}\right) \approx \frac{v}{V} \tag{2.8}$$

Equation 2.8 provides an appropriate approximation for small side-slip angles. Differentiating Equation 2.8, yields

$$\dot{\beta} = \frac{\dot{v}}{V} \tag{2.9}$$

Combining Equations 2.7 and 2.9 gives the general result for constant forward velocity as

$$a_y = V(r + \dot{\beta}) \tag{2.10}$$

Equation 2.10 shows the relationships between lateral acceleration, yaw rate, and $\dot{\beta}$.

Yaw rate is a direct function of the turn radius and vehicle speed, or $r = \rho V$. Given the yaw rate, a reduction in lateral acceleration, and hence curvature, produces a reduction in $\dot{\beta}$. Reducing curvature also reduces the yaw rate. This reinforces the hypothesis that these dynamic response effects can be minimized by reducing the curvature of the vehicle's path through the test course. Minimizing these dynamic effects improves the ability of the simulator or driver to effectively run the vehicle through the course. Additionally, the maximum test speed should increase due the elimination of unnecessary dynamics generated by suboptimal maneuvering.

2.2 Path Optimization

There are several different objectives for path optimization found in the literature. These include optimization of time, distance and driver comfort. In this research, an optimal path is defined as the path that best enhances the vehicle's ability to navigate a course with constraints. Therefore, the optimization objective was to obtain a vehicle path that reduced the vehicle dynamics during a test run. The benefits of minimizing the vehicle's dynamics include: creation of an objective and repeatable test, improved implementation on the Roadway Simulator and maximized vehicle test speed during the DLC maneuver.

Since many of the vehicle's dynamics are excited by lateral acceleration, these effects can be reduced by minimizing the lateral acceleration. However, lateral acceleration is a function of the vehicle's forward velocity. Using Equation 2.3 we can optimize a path by minimizing path curvature, and thus minimizing lateral acceleration.

The optimal path satisfies

$$\min_{\rho} \max_{1 \leq j \leq n} \{f_j(\rho)\} \qquad\qquad (2.11)$$

where $f_j(\rho)$ is the magnitude of the curvature $|\rho|$ at the jth point along the cg path subject to:

$$
\begin{aligned}
\text{Left Front Corner} &\leq \text{Upper Course Constraints} \\
\text{Left Rear Corner} &\leq \text{Upper Course Constraints} \\
\text{Right Front Corner} &\geq \text{Lower Course Constraints} \\
\text{Right Rear Corner} &\geq \text{Lower Course Constraints}
\end{aligned}
$$

The number (n) of functions $f_j(\rho)$ is dependent on the x spacing of the cg path. The variables defining the cg's path can be altered until the maximum of all the path curvature values is minimized subject to the vehicle's location within the course constraints.

A vehicle path optimization model was created to perform the operation described above, and is presented in Chapter Three. This model finds an optimal path from an infinite number of possibilities, ultimately reducing the dynamics that lead to vehicle spin-out and tip-up. The variables that determine the path's configuration and corresponding curvature are dependent upon the format of the model, as discussed in the next chapter.

Chapter 3

Vehicle Path Optimization Model Development

There are an infinite number of paths that could satisfy the requirements for the NATO DLC at a given speed. The goal was to develop a path optimization model that is adaptable to a variety of test vehicles and able to produce a repeatable and effectively optimal vehicle path. In this chapter, a vehicle path optimization model is developed using Microsoft Excel's Solver. This model is based on minimizing the maximum path curvature while maintaining the vehicle's position within the course boundaries.

3.1 Excel Solver and Its Optimization Routine

Microsoft Excel provided the ability to solve nonlinear constrained optimization problems, and was chosen because of its relative simplicity. The Excel Solver employs Generalized Reduced Gradient (GRG) optimization methods for solving nonlinear optimization problems. This is the basis for the GRG2 algorithm developed by Lasdon et al., which is discussed in detail in [19]. The GRG2 algorithm converts the optimization problem into a variable Jacobian matrix. The Jacobian matrix is obtained using finite difference approximations. Unlike linear optimiza-
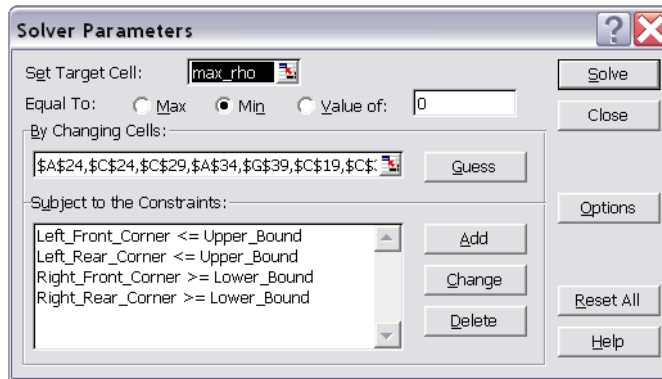
Figure 3.1: Microsoft Excel Solver Command Window

tion problems, the Jacobian matrix must be recalculated for each trial solution.

The GRG2 nonlinear optimization program was proven by Lasdon to be a robust solver in comparison to other gradient-based methods. However, the solver is limited to providing a locally optimal solution due to its gradient-based optimization technique. Additionally, a locally optimal solution is only guaranteed for a well defined problem.

Details of the solver's approach and additional optimization applications are discussed by Fylstra et al. in [5]. Fylstra provided a thorough discussion of the optimization methods used in the Excel Solver and its similarities with other spreadsheet solver programs. The Excel Solver designers recommended choosing appropriate initial starting values that are relatively close to the assumed optimal solution. Otherwise, the Solver could be unable to find an optimum solution or could produce a poorly optimized solution.

The optimization solver is used to minimize a target function by changing set parameters within a constrained optimization space as defined generally in Equation 2.11. The command window for this solver is shown in Figure 3.1. For the curvature minimization problem, the solver was used to minimize a cell charac-

30

terizing the maximum path curvature. This produced a Min-Max optimization routine. The discontinuous, or non-smooth, nature of Min-Max optimization further emphasized the requirement to provide the solver with a close guess to the optimal result at the start.

At the onset, there was concern that GRG optimization algorithms might have difficulties converging to reasonable results. However, it is shown in the following sections that the method was generally successful. Since the Min-Max optimization routine attempted to minimize the maximum curvature, it did not discriminate on curvature activity in the path with values less than the maximum curvature. Consequently, the optimization solutions are not unique and are probably only locally optimal. Nonetheless, the basic results were quite positive. It was also hypothesized that an optimal path should consist of a sequence of constant curvature sections. The results supported this argument, though a rigorous mathematical proof was not completed.

3.2   The Excel Solver Optimization Model

The NATO DLC test course configuration is shown graphically in Figure 1.2. For field tests traffic pylons mark the course, which is partially determined from the vehicle's dimensions. On the RWS, the pylon markers are simulated mathematically. Test vehicles initially enter the course at relatively low constant speeds. They are required to pass through section 1 parallel to the course boundaries. After leaving section 1, the driver is free to execute any steer input required to continue through the course at a constant forward velocity without exiting the course. The test is repeated at increasing speed increments, until either two wheel tip-up occurs, yaw instability occurs, or the vehicle can no longer increase in speed due to lack of

Table 3.1: NATO DLC Course Section Dimensions

Position in meters	Section 1	Section 2	Section 3	Section 4	Section 5
X_0	0	15	$39 + l$	$64 + l$	$68 + l$
X_{end}	15	$39 + l$	$64 + l$	$68 + l$	$103 + l$
Y_{lower}	0	0	3.5	0	0
Y_{upper}	$(1.1)w + .25$	$(1.2)w + 3.75$	$(1.2)w + 3.75$	$(1.2)w + 3.75$	$(1.1)w + .25$

$$l = \text{Vehicle length in meters}$$
$$w = \text{Vehicle width in meters}$$

power.

3.2.1 Vehicle Path Model Structure

The model was designed for easy adaptation to a variety of vehicle platforms, and required specific information about the test vehicle. This information included the vehicle's: width (w), length (l), cg location and transient body side-slip (or slip angle) characterization. The model discussed in this thesis uses the physical characteristics of a light-duty utility military tactical vehicle. The constraints of the path for the NATO DLC course were based on this vehicle. Table 3.1 summarizes the dimensions of the five sections of the NATO DLC maneuver displayed in Figure 1.2. The test requires the vehicle maintain a straight trajectory within section one of the course. The vehicle's heading orientation is unrestricted at the end of the test course.

The model defines the vehicle path based upon a number of finite points equally spaced in the longitudinal $(+x)$ direction. Each point represents the location of the vehicle's cg. The spacing distance, Δx, between each point was set to one meter. Decreasing this value improved the accuracy of the path model's calculations, but increased the time required to determine the optimal path. The grid spacing also affected the accuracy of the interpolation used to calculate the vehicle corner locations near the course constraints. The collection of all the path points represents the trajectory of the vehicle's cg. The lateral acceleration acting on the vehicle was calculated directly based on the vehicle path.

There are two primary components of the path which are calculated: the lateral acceleration at the vehicle's cg and the location of the vehicle's corners during the maneuver. Since the path is defined by a finite set of points, finite difference techniques were used to compute the lateral acceleration of the vehicle, as well as its orientation and the location of the vehicle's corners. A Taylor Series approximation was used to generate a centered finite difference approximation of the first and second derivatives of the path. The centered difference equations of the first and second derivatives are shown below in Equations 3.1 and 3.2, respectively. A centered difference scheme was utilized to reduce approximation errors generated in a one-sided forward or backward difference scheme. The first derivative was used to generate the slope of the vehicle at each location on the curve. The inverse tangent of this slope produced the course angle, which was based strictly upon the layout of the path.

The First Derivative approximation:

$$\frac{dy}{dx} = \frac{y_{j-1} + y_{j+1}}{2\Delta x} \tag{3.1}$$

The Second Derivative approximation:

$$\frac{d^2y}{dx^2} = \frac{y_{j-1} - 2y_j + y_{j+1}}{\Delta x^2} \tag{3.2}$$

where

$$y_{j-1} = y\ value\ of\ the\ preceding\ point$$

$$y_j = y\ value\ of\ the\ point\ of\ interest$$

$$y_{j+1} = y\ value\ of\ the\ following\ point$$

$$\Delta x = The\ fixed\ x\ difference\ between\ each\ of\ the\ points$$

For low-speed trials, a simplified side-slip model shown in Figure 2.3 was used to estimate body slip angle. For higher speed trials, the vehicle slip angle (or side-slip) was characterized from transient steering test results. Kefauver ([16]) from ATC's RWS facility used Matlab's system identification toolbox to estimate a dynamic model from RWS data. This model computes the vehicle slip angle from lateral acceleration as determined by the excel worksheet.

Combining the effects of the vehicle course angle and vehicle side-slip angle generated the vehicle's heading angle, ψ. This heading angle was used to calculate the location of the vehicle's corners with respect to the vehicle's cg location. The vehicle corner locations were calculated using rotational matrices as defined in Equation 3.3.

$$\begin{bmatrix} \mathbf{X_{corner}} \\ \mathbf{Y_{corner}} \end{bmatrix} = \begin{bmatrix} \cos\psi & -\sin\psi \\ \sin\psi & \cos\psi \end{bmatrix} \begin{bmatrix} \mathbf{x} \\ \mathbf{y} \end{bmatrix} + \begin{bmatrix} \mathbf{X_{cg}} \\ \mathbf{Y_{cg}} \end{bmatrix} \tag{3.3}$$

where

$$\mathbf{X}, \mathbf{Y} = Distance\ from\ the\ origin\ of\ the\ global\ coordinate\ system$$

$$\mathbf{x}, \mathbf{y} = Distance\ of\ the\ corner\ from\ the\ vehicle's\ cg$$

The second derivative of the discritized path was used in combination with the first derivative to determine the curvature of the vehicle path at each point based on Equation 3.4. Using Equations 2.3 and 3.4, the path's lateral acceleration was calculated given a constant forward velocity of the vehicle.

$$\rho = \frac{1}{R} = \frac{(1 + \frac{dy}{dx})^{\frac{3}{2}}}{\frac{d^2y}{dx^2}} \tag{3.4}$$

With the calculation of the curvature obtained for finite locations along the path, the value and location of the maximum curvature over the entire course was determined. A function was developed that determined the maximum absolute path curvature, with equal consideration to both positive and negative path curvature values. This was achieved in Excel by calculating the maximum path curvature from a column of absolute curvature values. The cell containing this value became the optimization solver's target cell for minimization.

The course constraints were a direct function of the vehicle's width and length as expressed in Table 3.1. The dimensions of the course prescribed the available solution space. Any path outside of the course boundaries resulted in a failed test. More specifically, if any corner of the vehicle exited the course boundaries, the result was a failed test. Therefore, it was necessary to develop a method to determine if the corners had satisfied the course boundaries. This required calculating the vehicle corner locations at or near the course boundaries.

Linear interpolation was used to determine the corner positions at the location of each course cone. Since this interpolation was applied to a curved path, the result produced a conservative estimate of the vehicle corner locations with respect to the course constraints. As the spacing between the course points were decreased, the corner estimations approached their actual values. However, decreasing the

spacing between the points increased the computational intensity of the program to potentially unnecessary levels. Assuming that the vehicle path was a perfect arc of constant radius starting at a given point a and ending at point b, a linear approximation of this arc would contain the most error if points a and b were equidistant from the point of interpolation. Therefore, if the arc radius of the path was greater than 90 meters, a 1 meter spacing between points a and b, would produce an error of less than 1.39 mm. This error was considered negligible in our model. It is shown later that the NATO DLC course does not generate an arc radius of less than 94 meters, thus ensuring that the calculation error does not exceed 1.39 mm.

The course constraints were then applied to the vehicle path optimization model. Each vehicle corner was constrained within the limits of the course boundaries shown in Figure 3.2. The space defined by the course boundaries represented the potential solution space. Excel's Solver was limited for the number of constraints allowed, which presented a problem due to the number of upper and lower course constraints. Therefore, the number of the constraints was reduced by requiring that the right vehicle corner y-values were greater than or equal to the lower course constraints. Likewise, the left vehicle corner y-values were restricted to being less than or equal to the upper course constraints.

3.2.2   Early Implementation

Through predefining the x locations for each of the cg location points, a fixed Δx was maintained. The y locations of the cg points were defined as the "changing cells" within the Excel Solver. The Solver was able to vary the y-value for each cg point with the constraint of the course boundaries while minimizing the curvature
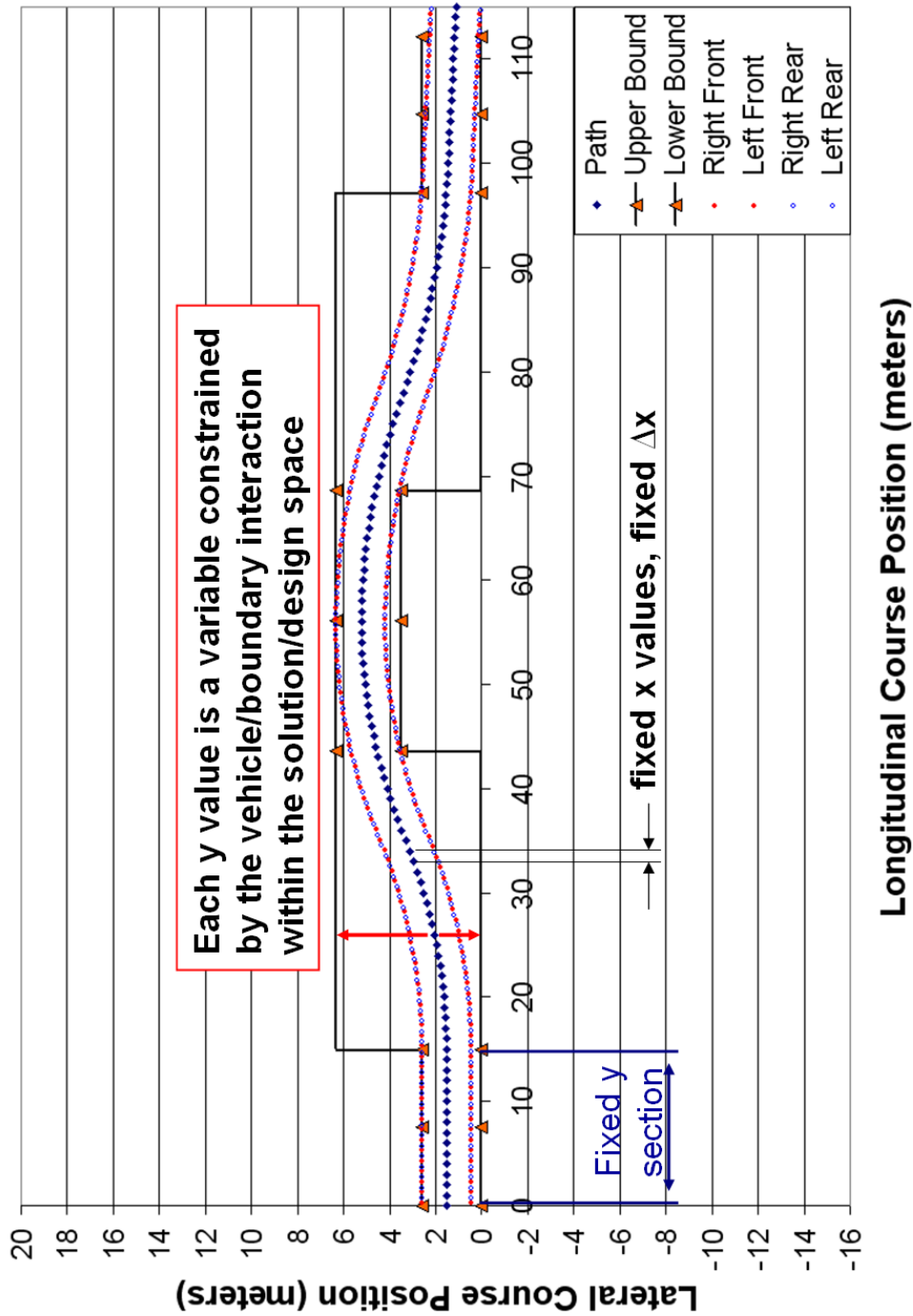
Figure 3.2: Microsoft Excel Vehicle Path Configuration

of the vehicle's path. Since each cg y-value was variable in the Excel Solver, optimization became calculation-intensive, and was sensitive to grid spacing of the points and the initial path guess.

Early optimization work conducted with the Excel Solver lacked repeatability and convergence. The convergence to an optimal trajectory was highly dependent upon the initial path provided to the Solver. Based on intuition, path solutions that generated curvature values less than .015 (m^{-1}) were considered possible solutions, allowing diverging results to be eliminated from further study.

Several characteristics were discovered about the path optimization process. The successful optimization solutions were characterized by plateaus of constant curvature values over the curved regions of the course. This phenomenon led to the hypothesis that the path with the minimum maximum curvature values would be composed of constant radius arcs and possible straight segments.

Figures 3.3 through 3.6 display vehicle path plots and absolute curvature plots for Δx of 2.43 meters and 1.215 meters, respectively. The constant curvature plateaus are clearly displayed in Figures 3.4 and 3.6. The spikes indicated a difficulty for the model to locally minimize the maximum curvature values. This was due to the non-smooth optimization characteristics of a Min-Max optimization routine. It was due to the result that the optimization routine did not discriminate curvature activity less than the maximum value. As shown in Figure 3.6, doubling the number of path points reduced the Solver's ability to reproduce the relatively smooth curvature plateaus present in Figure 3.4.

Additional improvements to the model included the use of a variable cushion space between the course boundaries and the design space of the vehicle path to ensure successful implementation on the Roadway Simulator.
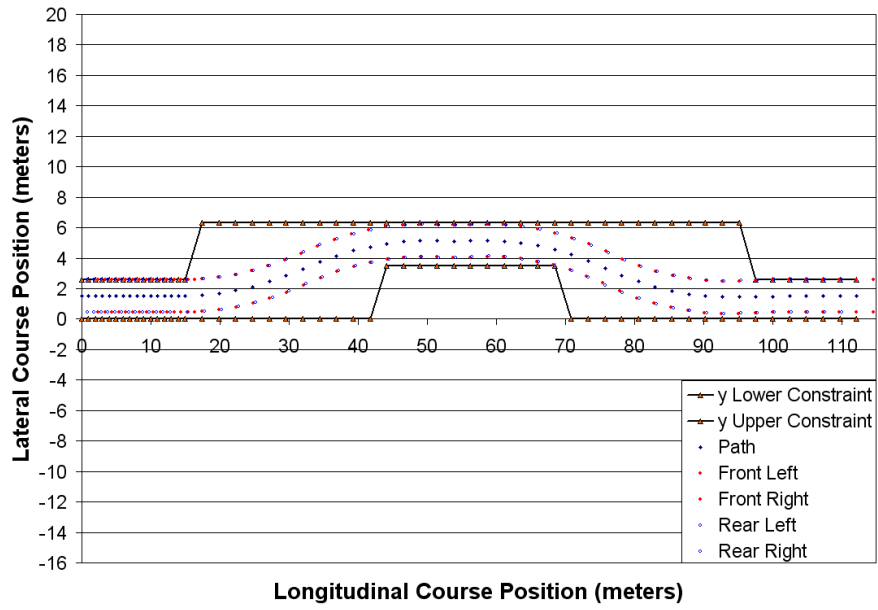
Figure 3.3: Vehicle Path for $\Delta x = 2.43$ meters

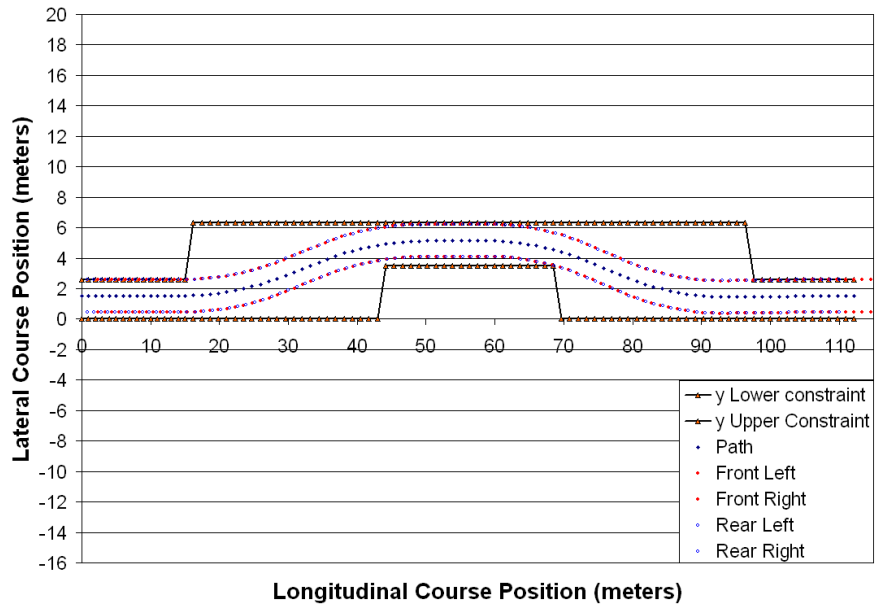Figure 3.4: Path Curvature for $\Delta x = 2.43$ meters

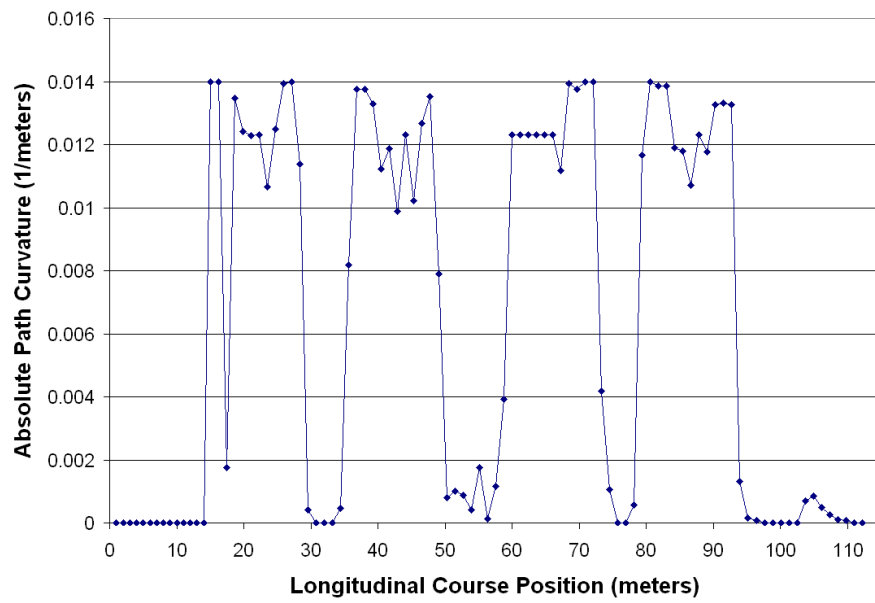Figure 3.5: Vehicle Path for $\Delta x = 1.215$ meters

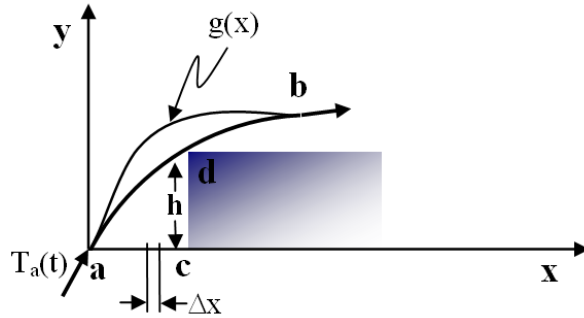Figure 3.6: Path Curvature for $\Delta x = 1.215$ meters

Figure 3.7: Argument Illustration for Constant Radius Segments

3.3 Optimization with Constant Radius Arcs

As mentioned earlier, it seemed intuitive that the optimal path should consist of a series of constant curvature segments with possible straight segments between them.

3.3.1 Argument for Constant Radius segments

Consider two arbitrary points a and b along a trajectory from point a to point b with an obstacle between them as shown in Figure 3.7. Let $g(x)$, the path, be expressed parametrically by a vector valued function,

$$R(t) = x(t)\hat{i} + y(t)\hat{j} \qquad (3.5)$$

Assume at first that the path heading (tangent to the curve) at point a lies on the circle arc segment connecting points a,b and d. We are searching for a curve $g(x)$ or $R(t)$ that is continuous and differentiable from a to b with the minimum peak (maximum) curvature, subject to the constraints $y(c) \geq h$ and the unit tangent at a $(T_a(t))$ lies on the circle given by a, b and d. The unit tangent is given by

41

$$T(t) = \frac{\frac{dR(t)}{dt}}{\left|\frac{dR(t)}{dt}\right|} \tag{3.6}$$

By definition, curvature is given by

$$K(t) = curvature = \frac{\frac{dT(t)}{dt}}{\left|\frac{dT(t)}{dt}\right|} = \left|\frac{\frac{dT(t)}{dt}}{\left|\frac{dT(t)}{dt}\right|}\right| \tag{3.7}$$

If time t is discretized by Δt and we let t_0 be at a, then at t_0 any curve that starts out with $K(t) > K(circle)$ (given by the circle with points a,b and d) is automatically excluded from the search. Similarly any curve that starts out with a $K(t) < K(circle)$ (i.e. on a larger radius circle) and then steers back towards the original circle with $K(t) > K(circle)$ is also immediately excluded. Any curve that starts out with $K(t) < K(circle)$ and then steers back with $K(t) = K(circle)$ will never reach point b. By discretizing t from t_0 (at a) to t_f (at b) and applying the above argument, it can be shown that the path with the minimum maximum curvature from a to b subject to the stated constraints is the constant radius curve given by points a,b and d. This result is intuitive. Part of the challenge is adequately defining the constraints. One could argue for a trajectory that proceeds in a counterclockwise manner from a to b. However, this would produce an implausible result for the DLC test.

Based on this intuitive result, it seemed that the optimum path through the entire DLC course should consist of a sequence of constant curvature segments with possible straight sections joining one or more of the curved segments as shown in Figure 3.8. A attempt was made to use the principles of optimality and dynamic programming to provide a mathematical proof to this idea. However, the non-continuous nature of the curvature function when transitioning from section to section disallowed this approach in any strict sense. A rigorous mathematical

proof was not completed in this research and a formal mathematical proof is left for future work.

Alternatively, the hypothesis was demonstrated using the optimization model described in this chapter. To converge on this result, it was first necessary to assume that the optimal path was composed of six or nine constant curvature and straight segments as described in the following sections. The optimal paths generated with these assumptions were then used as starting points for a general search of the solution space with the model as described in sections 3.2.1 and 3.2.2. In other words, the constant curvature segment constraints were relaxed after a solution was found with constant curvature segments. The general optimization was then executed. As will be shown at the end of this chapter, the intuitive argument for the construction of an optimal path consisting of constant curvature segments was demonstrated to be true for at least a locally optimized solution.

3.3.2   A Constrained Six-Segment Path Model

Based upon the constant radius sections displayed in Figures 3.4 and 3.6, the course was divided into six segments of curves. The path producing these segments of curves is presented in Figure 3.8. The first segment was prescribed by the NATO DLC as parallel to the course's longitudinal axis. At $x = 15$ meters, the path was free to enter the region of the first arc, which was concave up. Midway into section two of the course, the vehicle reached a point of inflection where the second arc began, which was concave down. Midway into section three of the course, the vehicle began the third arc segment (also concave down). In section four of the course, another inflection point occurred as the fourth arc is initiated (concave up). This final arc ended with a straight section. For simplicity, the final straight
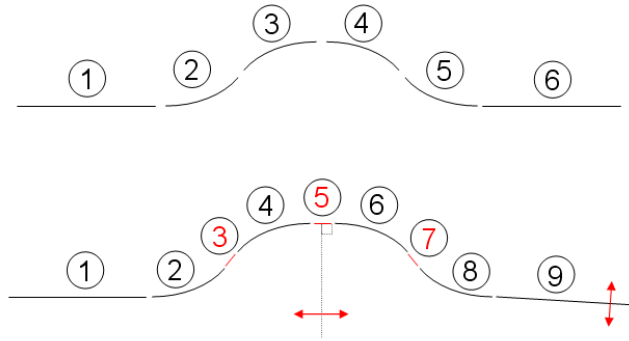
Figure 3.8: Vehicle Paths Composed of Six and Nine Curve Segments

section was forced to remain parallel to the longitudinal axis of the course, similar to the initial straight section. An additional simplification constrained the course heading angle at the intersection of arc two and arc three (section three and four for the six-segment path) to be parallel to the longitudinal axis of the course.

The end conditions of each segment were matched for continuity. A thorough description of the required relationships and the necessary calculations for each curve are given in Appendix A.1. The result was a path with seven primary variables listed in A.1.2, which were used to determine the y-values for each of the six segments listed in A.1.4. This produced a substantial reduction in the number of changing cells within the Solver from the initial implementation, which required in excess of 100 changing cells.

Implementing the curve equations for each segment required the generation of an "if" statement in the model. The seven primary variables and their additional relationships (A.1.3) determined the locations of the starting and ending points for each of the six curve segments. The "if" statement applied the proper y-value equation at each x_i location along the path. The implementation of the "if"

statement provided flexibility for the path to change appropriately as the seven primary variables were changed.

The seven primary variables were responsible for the configuration of the vehicle path. Therefore, these variables had to be properly determined to reduce the overall path curvature. The Excel Solver appropriately changed these seven variables while seeking to minimize the path curvature. The optimization constraints and target cell were unchanged from the earlier model. The model produced the optimal segment arc radii and segment transition points. Figure 3.9 and 3.10 represent the vehicle path and path curvature, respectively, generated by the six-segment curve model at zero forward speed. The maximum curvature of the path was $\rho = .008737\ m^{-1}$ located over the first and second arc, corresponding to a path radius of 114.47 meters.
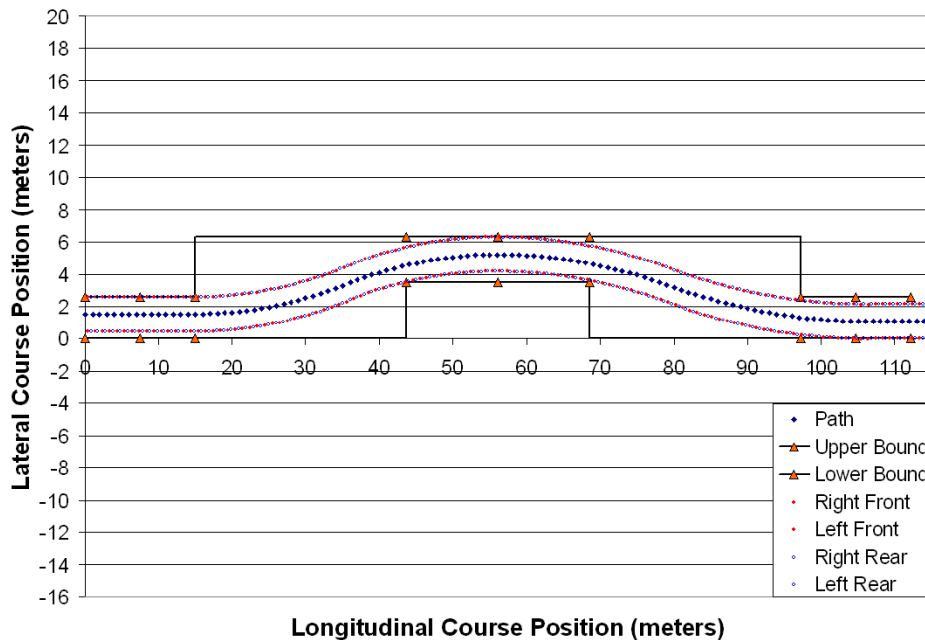

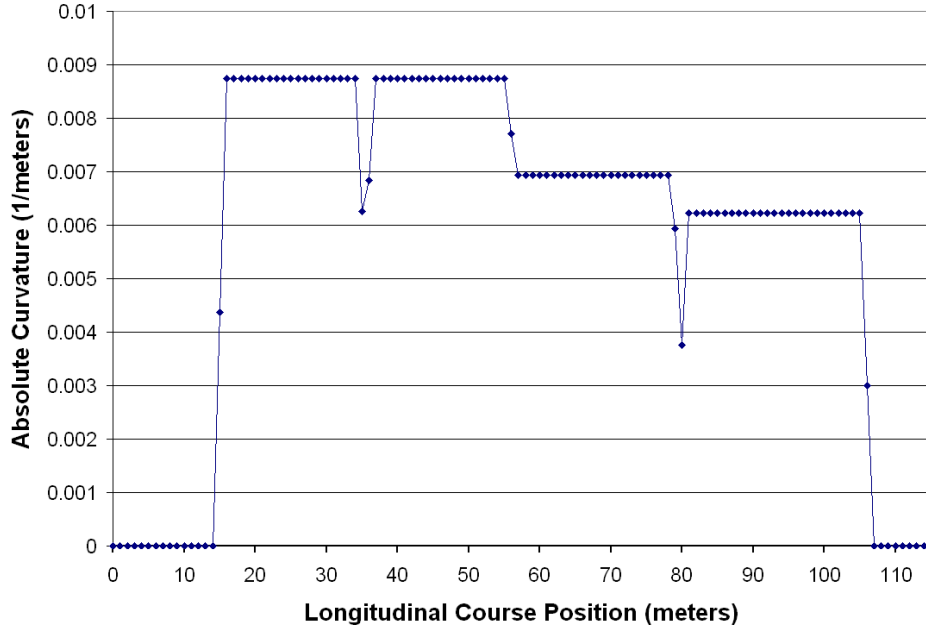Figure 3.9: Vehicle Path Generated by Six Segments of Constant Curvature

Figure 3.10: Absolute Curvature Values for a Six-Segment Vehicle Path

Starting with this solution, the constant curvature segment constraint was removed and the general optimization algorithm (from section 3.2.1) was executed. Each cg location point of Figure 3.9 was free to vary laterally. Figures 3.11 and 3.12 display the path and curvature values of the optimized result for the unconstrained model. The variation between Figure 3.9 and Figure 3.11 is small and best shown as an absolute lateral difference between the two paths. The absolute lateral difference plot is displayed in Figure 3.13. The differences were considered insignificant. The maximum curvature of the path was improved by only $3.12E^{-13}$ m^{-1}.

The results discussed in this section provide the initial verification of the argument for constant curvature segments. However, in the six-segment path model, assumptions were used to simplify the problem definition and reduce the available
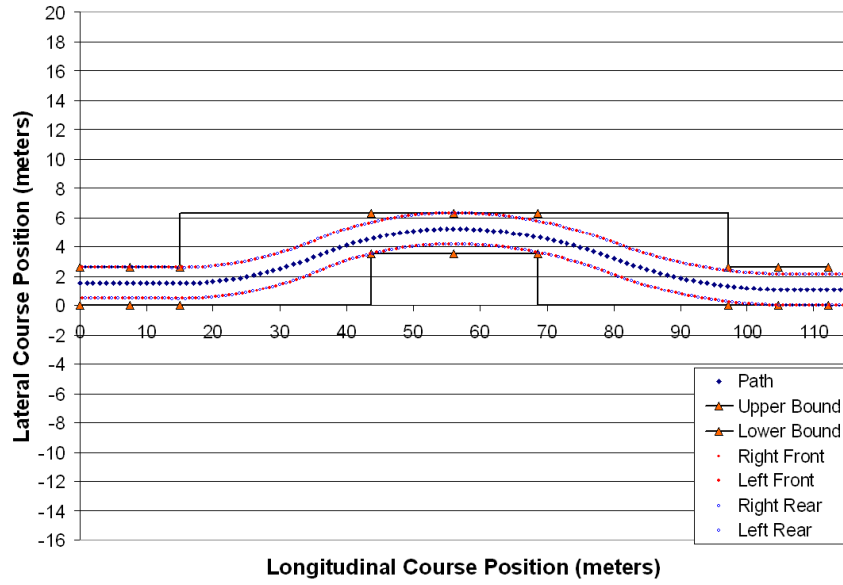
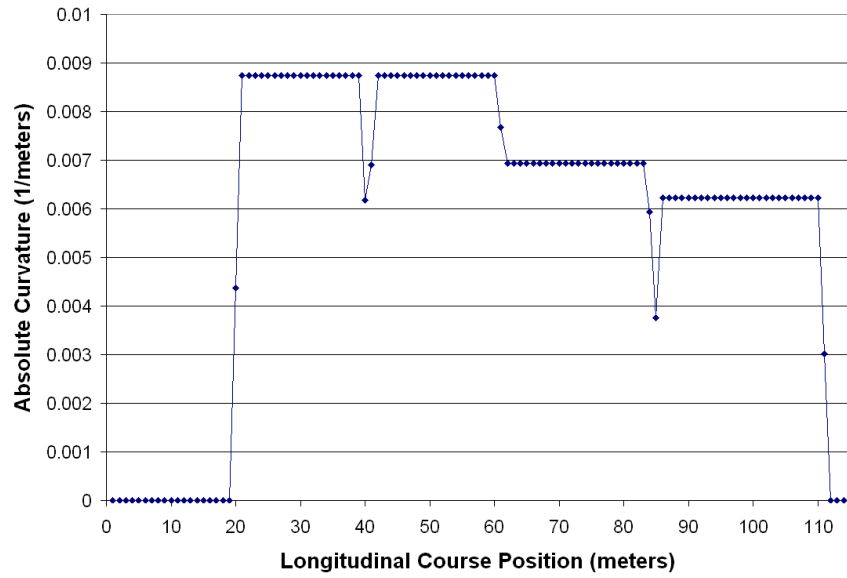Figure 3.11: Unconstrained Vehicle Path Using the Six-Segment Path

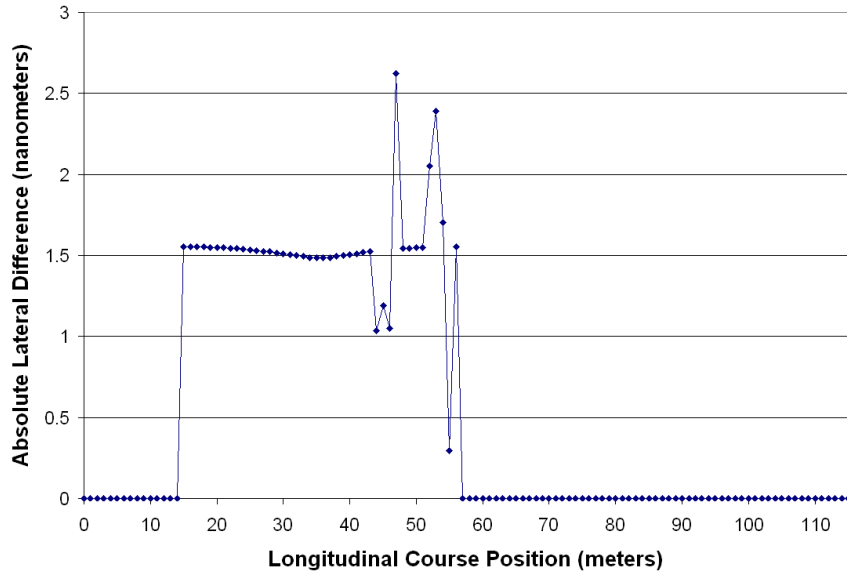Figure 3.12: Absolute Curvature for the Unconstrained Six-Segment Path

47

Figure 3.13: Lateral Difference Between the Six-Segment and Unconstrained Paths

solution space. A more general model is described next.

3.3.3   A Constrained Nine-Segment Path Model

A nine-segment curve model improved upon the six-segment model. Improvements included: an unrestricted vehicle heading angle between arc two and three, an unrestricted final vehicle heading angle, and three additional straight segments located at the transition points of each of the arcs. The basic format of this configuration is displayed in Figure 3.8. Detailed calculations and relationships enabling the end conditions of each neighboring segment to match continuously are discussed in Appendix A.2. The nine-segment model required 12 primary variables (A.2.2) to generate of the vehicle's path. Similar to the six-segment model, the 12 primary variables of the nine-segment model were used to determine the y-values for each segment of the curve. The necessary relationship and y-value equations

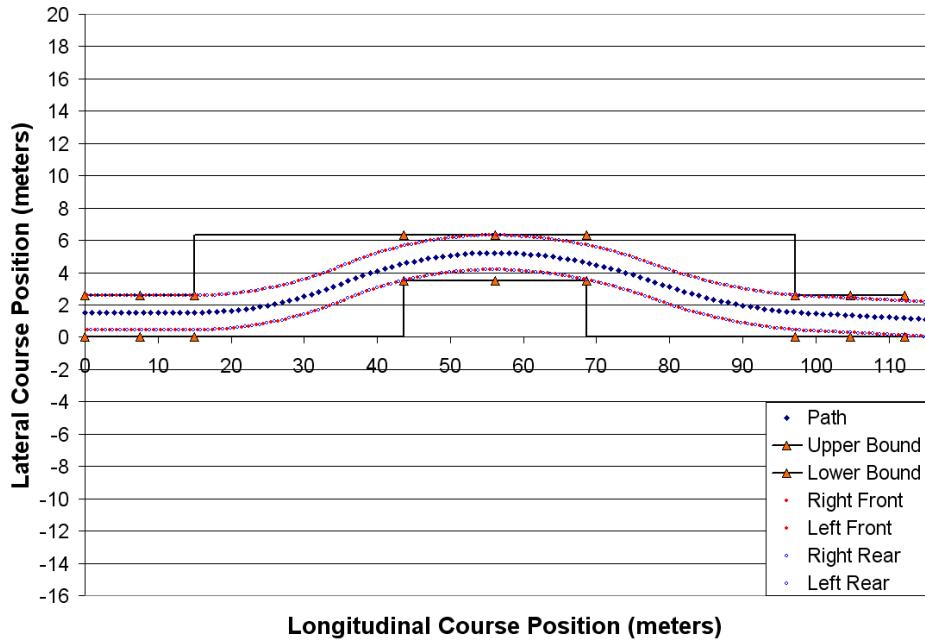for each segment are defined in A.2.3 and A.2.4.

Figure 3.14: Vehicle Path Generated by Nine Segments of Constant Curvature

The path produced by the nine-segment model is displayed in Figure 3.14. The corresponding absolute curvature plot is displayed in Figure 3.15 for zero forward vehicle speed. The nine-segment model generated a maximum curvature of $\rho = 0.00874\ m^{-1}$. Again, the region of maximum curvature was located equally through the first and second path arcs. This curvature was equivalent to a vehicle path radius of 114.46 meters. The maximum curvature of this model was essentially equal to value obtained in the six-segment curve. However, the nine-segment curve provided improved flexibility toward course boundary configuration changes.

The nine-segment curve model introduced three straight line segments between the original four curved segments of the six-segment model. The length of these line segments was measured as $d_{1,2}$, $d_{2,3}$ and $d_{3,4}$. The subscript designates the
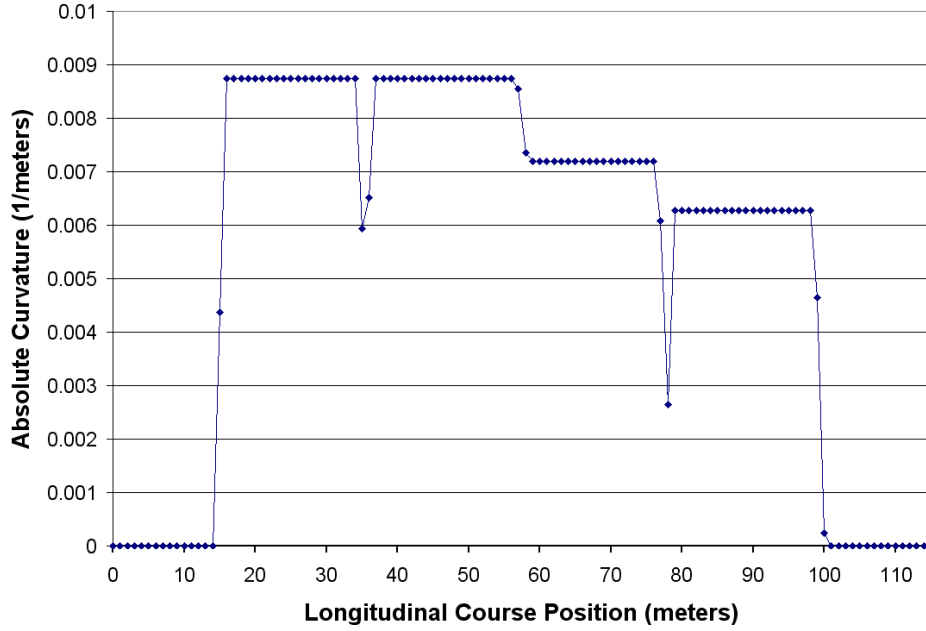
49

Figure 3.15: Absolute Curvature Values for a Nine-Segment Vehicle Path

arcs each line is located between. The optimal path produced by the nine-segment model resulted in $d_{1,2} = 0$ meters, $d_{2,3} = .509$ meters and $d_{3,4} = 0$ meters. The short length of these segments further verified that the optimal result was that of a sequence of constant curvature path segments. Though straight sections $d_{1,2}$ and $d_{3,4}$ were shown to be unnecessary at all speeds, as discussed in Chapter Four, the center straight section $d_{2,3}$ was a valuable segment within the model. This is also demonstrated further in Chapter Four. Therefore, it is possible to simplify the nine-segment model into seven segments for future implementation. However, for the remainder of this thesis the nine-segment model was retained.

As with the six-segment model, the nine-segment constant curvature result was used as the starting point for the general unconstrained model. This allowed the unconstrained model to determine whether the optimal path generated by the nine-
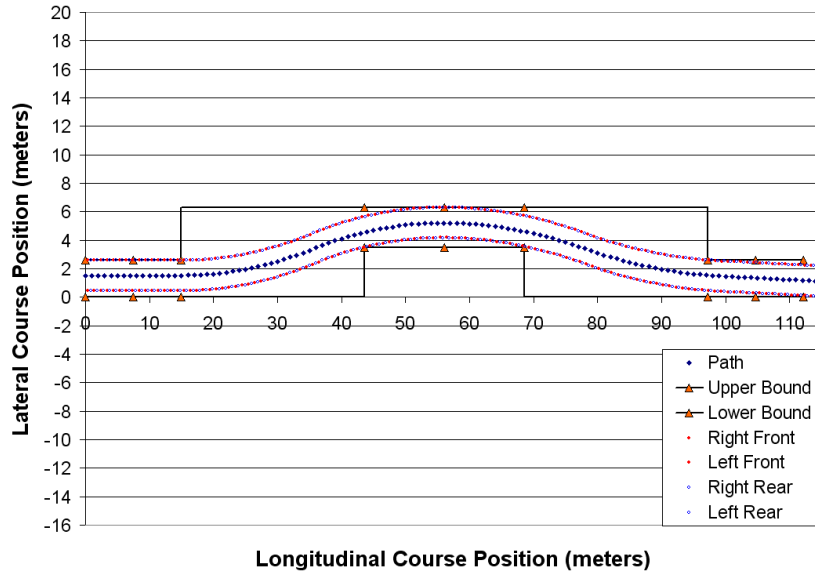
50

Figure 3.16: Unconstrained Vehicle Path Using the Nine-Segment Path

segment model could be improved upon. The vehicle path and curvature plots for the unconstrained model are displayed in Figures 3.16 and 3.17, respectively. The improvement made by the unconstrained model versus the initial nine-segment model path is illustrated in Figure 3.18, and was again insignificant. This result further strengthened the argument for constant curvature and straight segments.

3.4   Concluding Remarks on the Optimization Model

The nine-segment model was chosen as the primary path optimization model for this research due to its more general nature and flexibility. It removed the restraint placed upon the mid-course and final-course vehicle heading angles. It also showed that the straight sections between the first and second arcs and the third and fourth arcs were unnecessary. The straight segment between the second and third
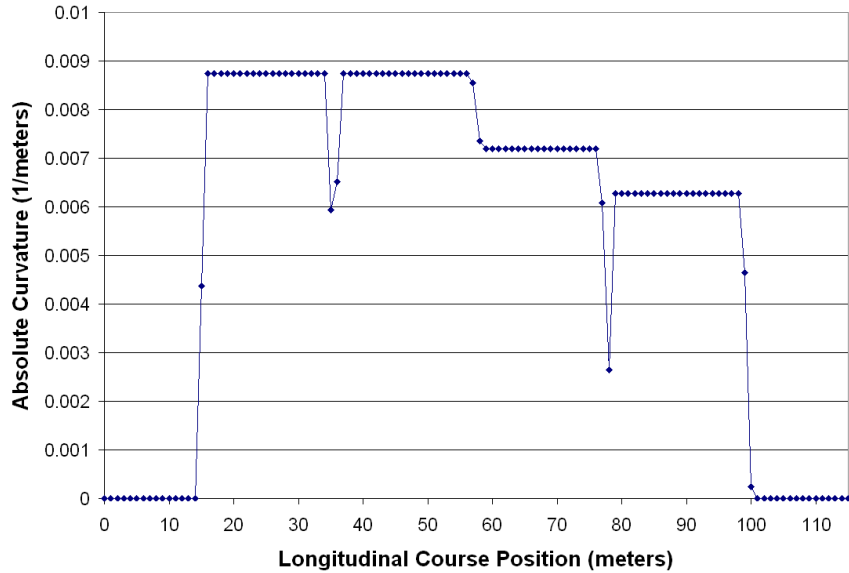
Figure 3.17: Absolute Curvature for the Unconstrained Nine-Segment Path

arcs was potentially significant as will be shown in Chapter Four.

The nine-segment path model using constant radius and straight segments appeared to produce at least a locally-optimized vehicle path. The inclusion of straight segments between the curved sections allowed the path to effectively stretch when needed without adversely affecting other path segments.

The path produced by the nine-segment model is not a uniquely optimal solution to the given course constraints. This is due in part to the effects of the Min-Max optimization routine. The Min-Max routine attempted to minimize the maximum curvature values in the path, but did not discriminate path activity with curvature less than the maximum curvature. Therefore, segments with lower curvature values are able to vary slightly without altering the maximum path curvature. Nonetheless, this superfluous activity did not improve or degrade the path generation
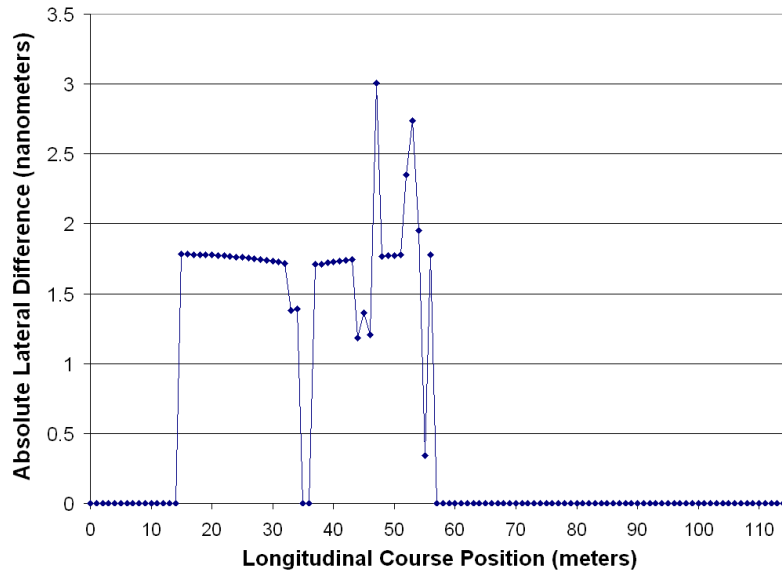
Figure 3.18: Lateral Difference Between the Nine-Segment and Unconstrained Paths

The lack of symmetry in the NATO DLC forced the maximum curvature to occur within the first two curved segments. This was due to the constraint that the vehicle remained parallel to the longitudinal course axis in the first section, while the vehicle heading angle was unconstrained in the last section of the course. The Min-Max routine focused on minimizing the curvature values in the first two curved segments while ignoring the curvature in the final two curved segments. The final two curved segments were free to vary within the course constraints until they affected the maximum path curvature or obtained values of curvature greater the current maximum path curvature. Since the end of the path is able to vary slightly without affecting the maximum path curvature, many paths could produce the same minimized maximum curvature values. Therefore, the path produced by the nine-segment model is not a unique result.

Chapter 4

Vehicle Path Optimization Model Testing

This chapter presents the results for the nine-segment path optimization model for a variety of vehicle speeds using a 2-axle light-utility military tactical vehicle. The test vehicle's length was 4.6 meters, and width was 2.13 meters. Each path result was generated as an optimal vehicle path given the specific test speed. Afterwards, the model results were compared to field test data and Roadway Simulator test results for the same basic vehicle.

4.1   Speed-Dependent Model Outputs

A zero-speed path, illustrated in Figure 3.14, was used as the base model for the speed trials. Iterations were run from 0 to 72.4 km/hr (45 mph) at increments of .8 km/hr (.5 mph). The starting path for each optimization trial was the optimal path from the next lowest speed. Figures 4.1 to 4.9 display the vehicle paths for vehicle testing speeds at 8.05 km/hr (5 mph) increments. The optimal cg trajectories for each speed are compared in Figures 4.10 and 4.11. The cg paths did not vary discernably until the vehicle reached approximately 56.3 km/hr (35 mph), where vehicle lateral acceleration and side-slip values became relatively large. Note that

lateral acceleration increases with the square of the vehicle speed.

At higher test speeds, it was also easier to discern differences in corner locations, again due to higher side-slip. Figure 4.10 illustrates the similarities of the paths from 8 km/hr (5 mph) to 48.3 km/hr (30 mph) in the first two turns. Since peak lateral acceleration was achieved in the first half of the path, the solver probably did not completely optimize the second half of the path. Thus, the results of the second half of the path are less consistent. Figure 4.11 illustrates the path differences between the three highest speed trials, showing that the cg trajectory moves further from the course cones as the speed was increased. This was caused by the increase in the vehicle side-slip. The lateral acceleration plots corresponding to each vehicle test speed are shown in Figures 4.12 to 4.20.

The length of the line segments between each arc in the nine-segment model is displayed in Table 4.4. The distance of the line segments between the first and second arc ($d_{1,2}$), and between the third and fourth arc ($d_{3,4}$) were zero for all test speeds. This result provided evidence that these sections could be eliminated from the model, producing a seven-segment model. It is also interesting to note the increase in the center straight segment length ($d_{2,3}$)as the speed was increased. The length of the straight segment is not discernable until it becomes greater than the 1 meter grid spacing. However, the model is able to calculate the appropriate length of the line segment.

Figures 4.21, 4.22 and 4.23 show the dynamic side-slip response of the vehicle calculated for 56.3, 64.4 and 72.4 km/hr (35, 40 and 45 mph) trials, using the dynamic model developed by Kefauver. For comparison, these results were plotted against side-slip estimates from the low-speed polynomial model displayed in Figure 2.3. These results highlight the need for the high-speed transient model of
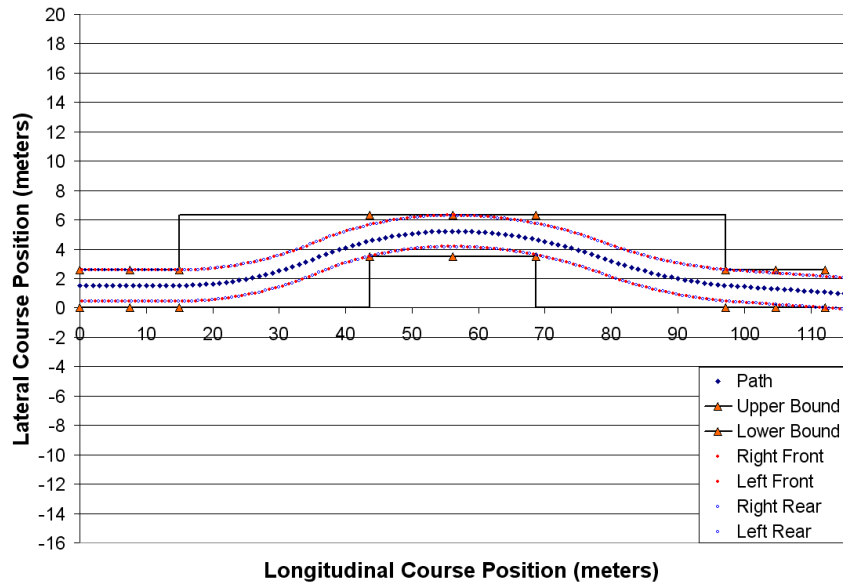
55

Figure 4.1: 8 km/hr (5 mph) Vehicle Path

side-slip for speeds at or exceeding 56.3 km/hr (35 mph). Vehicle speeds less than 56.3 km/hr (35 mph) did not generate enough activity in lateral acceleration to necessitate the use of this dynamic side-slip model.

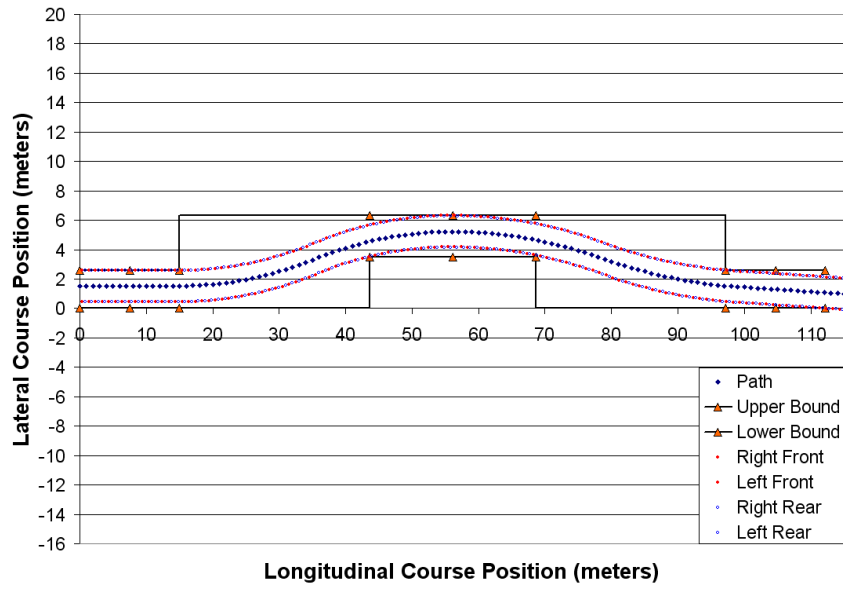The results from the speed paths are summarized in Tables 4.1, 4.2, 4.3 and 4.4.

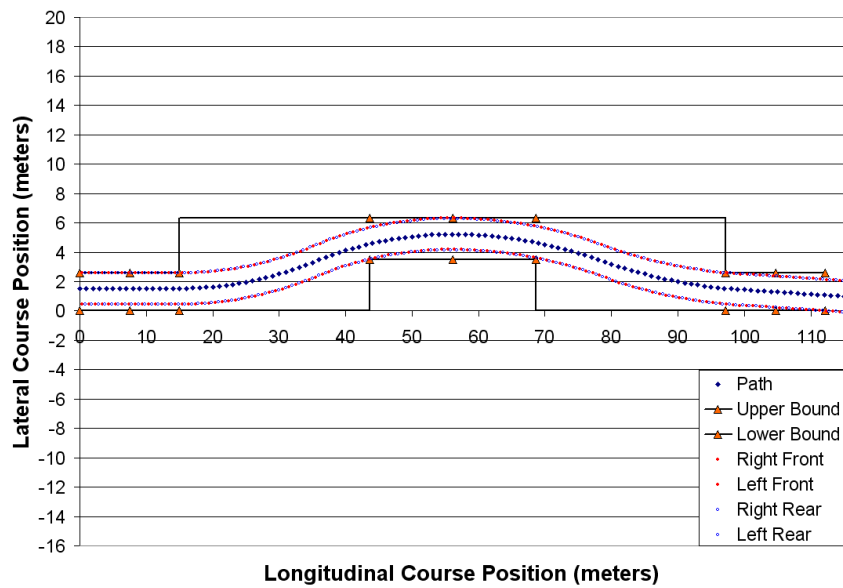Figure 4.2: 16.1 km/hr (10 mph) Vehicle Path
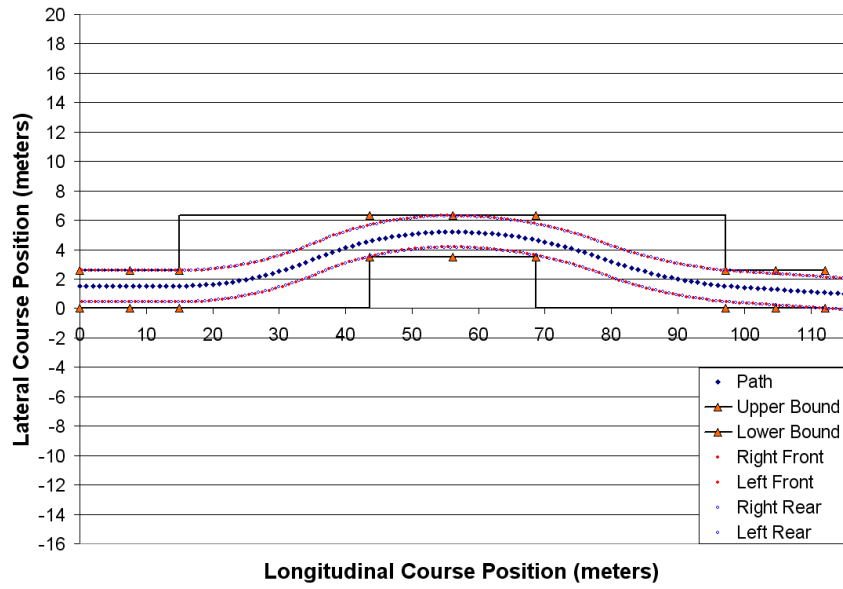

Figure 4.3: 24.1 km/hr (15 mph) Vehicle Path

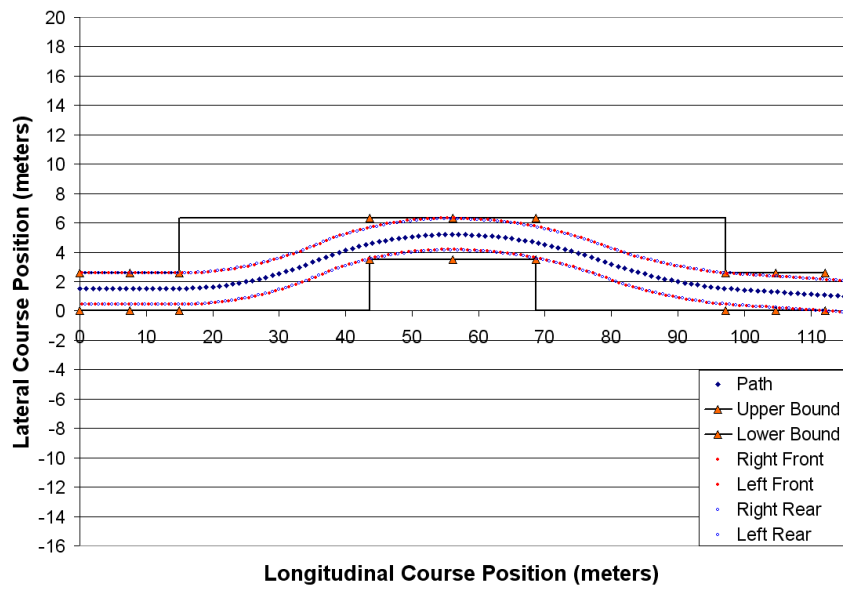Figure 4.4: 32.2 km/hr (20 mph) Vehicle Path

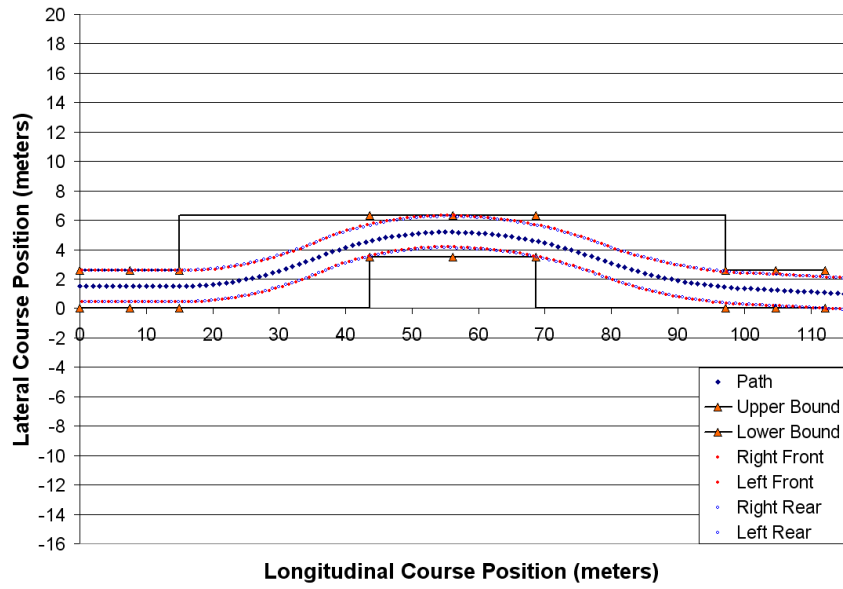Figure 4.5: 40.2 km/hr (25 mph) Vehicle Path

58
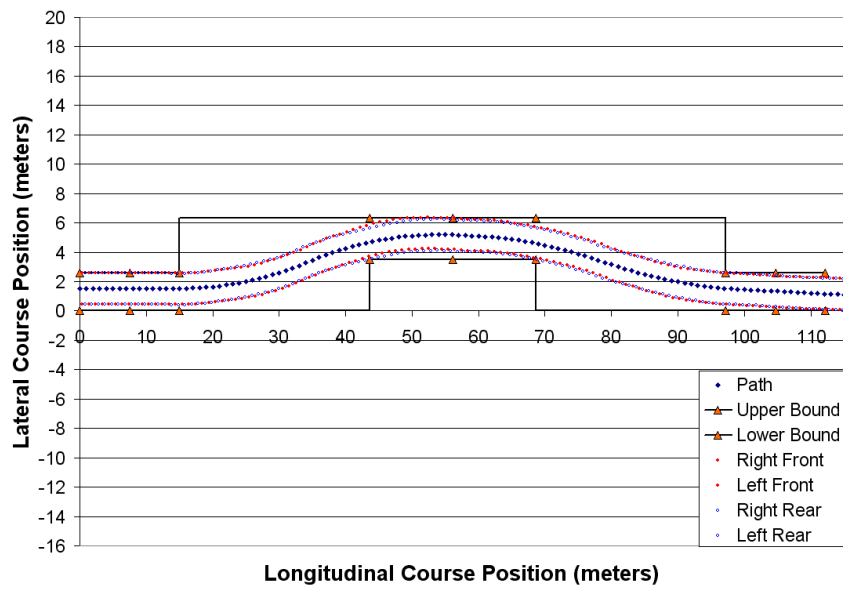
Figure 4.6: 48.3 km/hr (30 mph) Vehicle Path

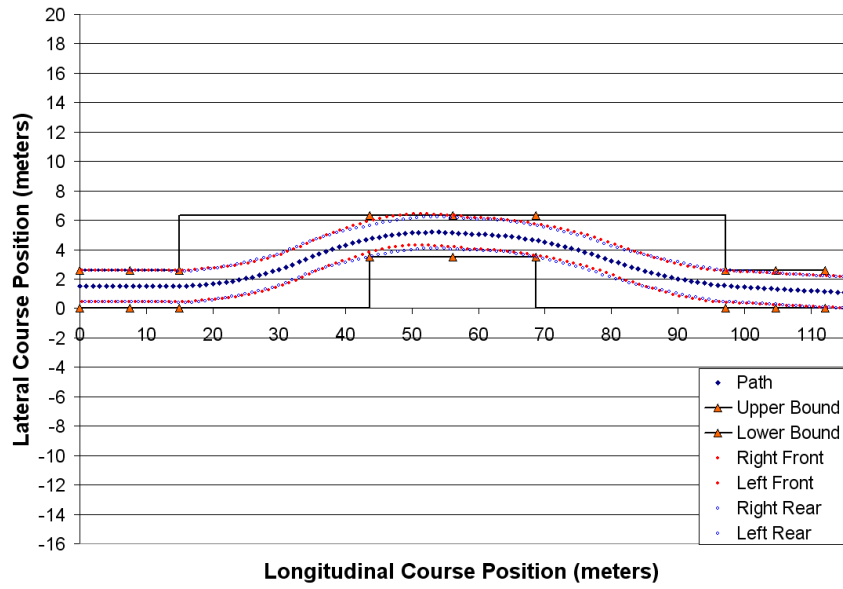Figure 4.7: 56.3 km/hr (35 mph) Vehicle Path

Figure 4.8: 64.4 km/hr (40 mph) Vehicle Path
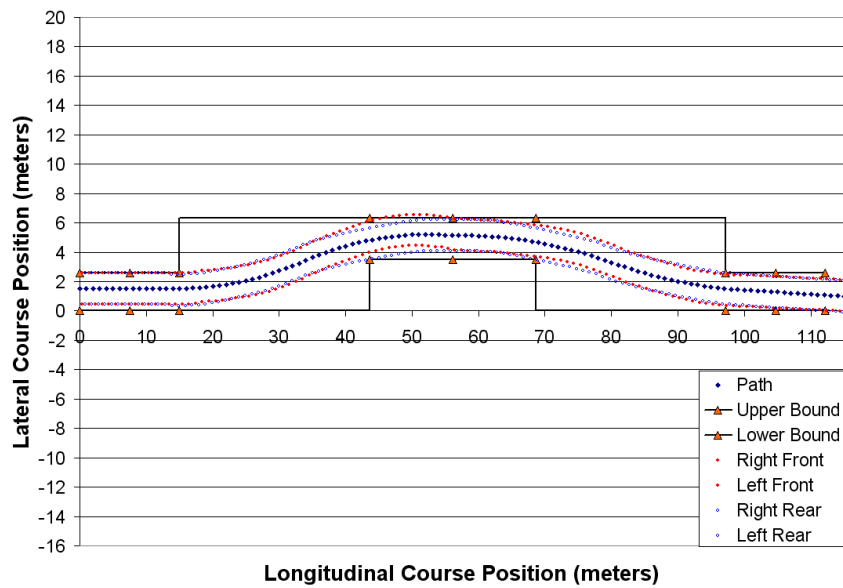
Figure 4.9: 72.4 km/hr (45 mph) Vehicle Path
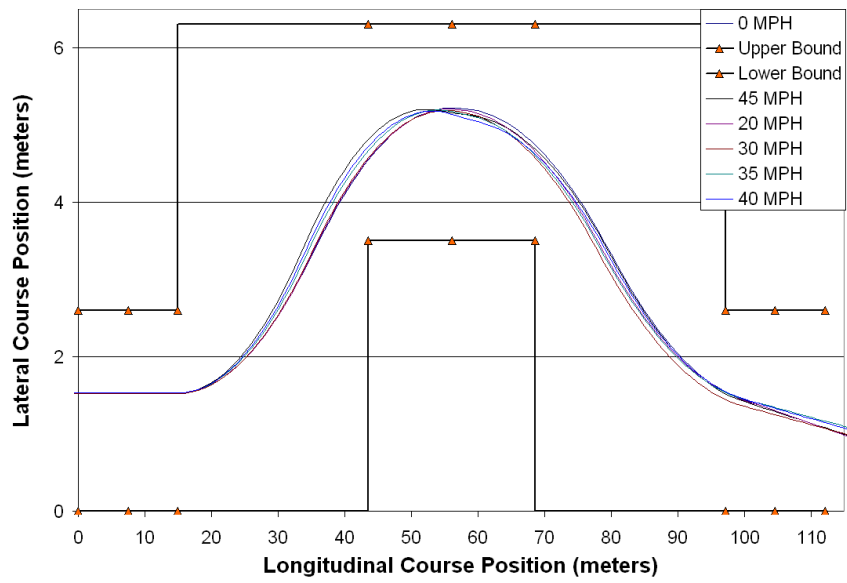
Figure 4.10: CG paths for multiple test speed values
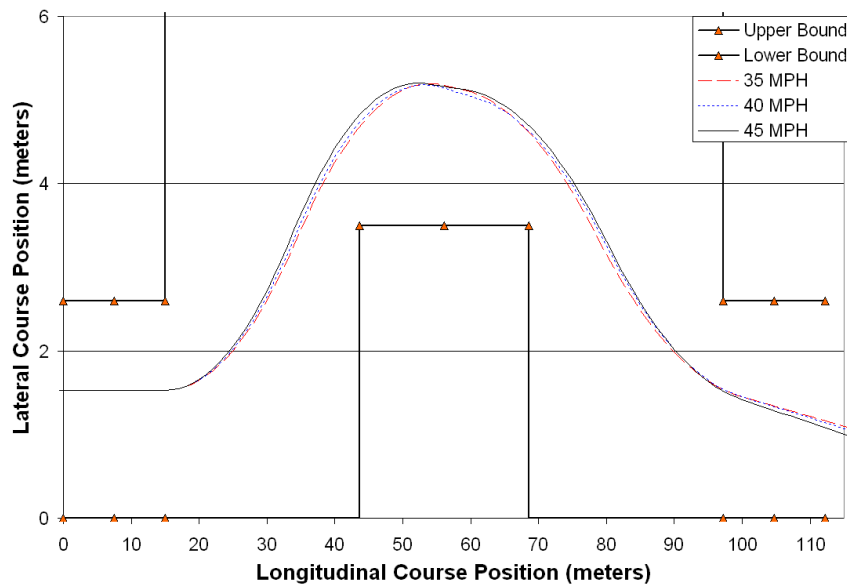
Figure 4.11: CG paths for 35, 40 and 45 MPH

Figure 4.12: 8 km/hr (5 mph) Lateral Acceleration Plot

Figure 4.13: 16.1 km/hr (10 mph) Lateral Acceleration Plot
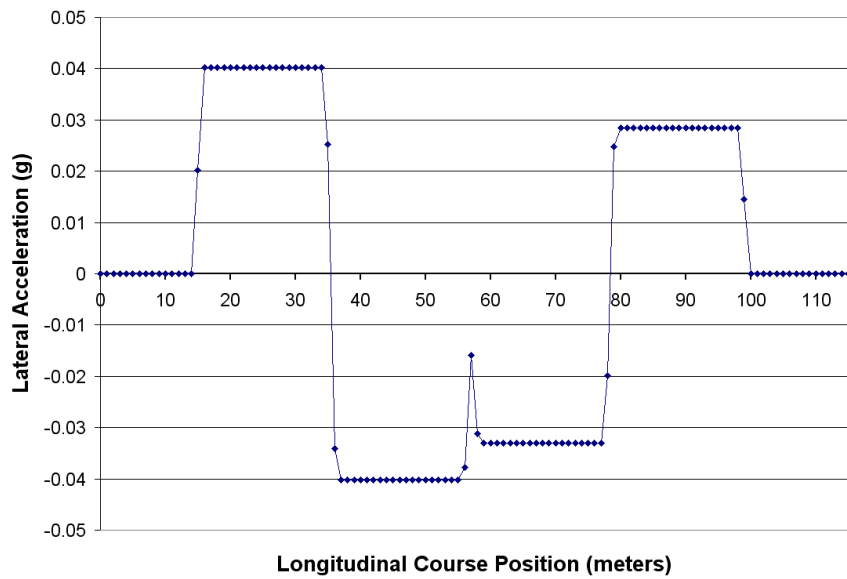
Figure 4.14: 24.1 km/hr (15 mph) Lateral Acceleration Plot
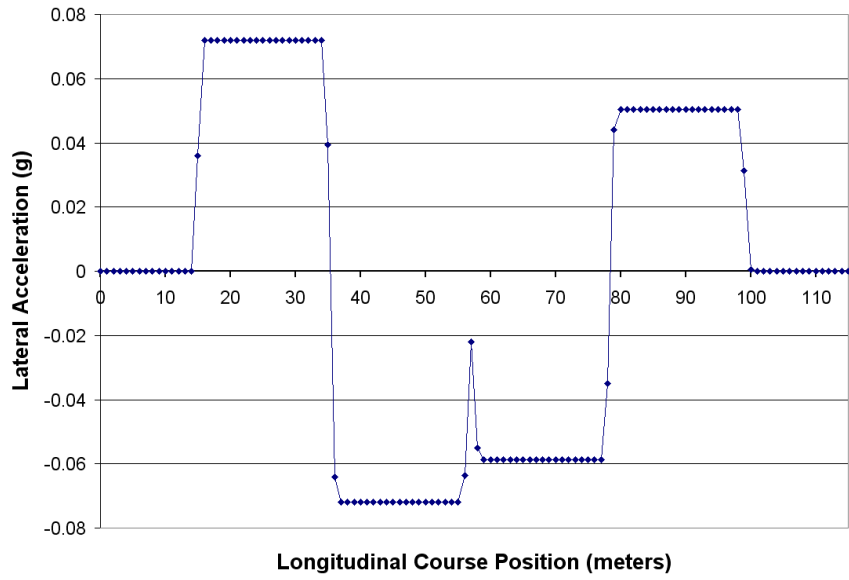
Figure 4.15: 32.2 km/hr (20 mph) Lateral Acceleration Plot
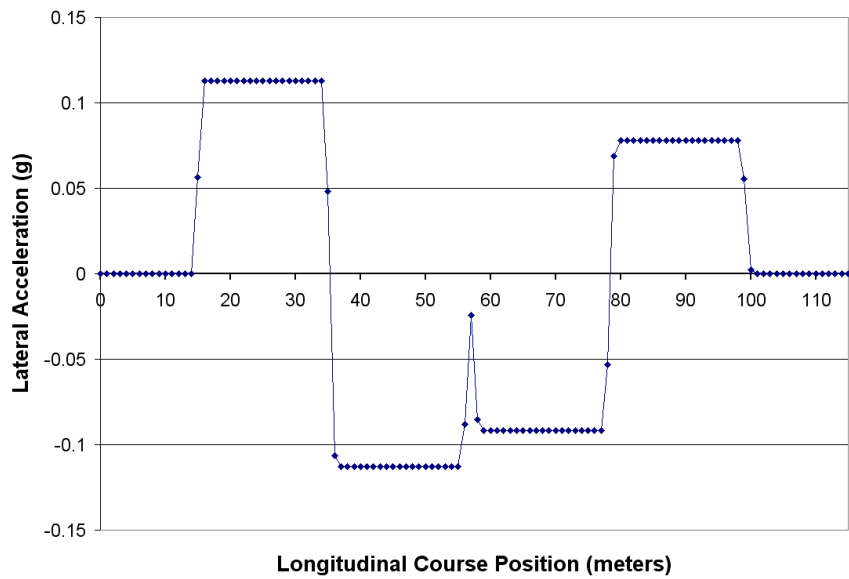
Figure 4.16: 40.2 km/hr (25 mph) Lateral Acceleration Plot
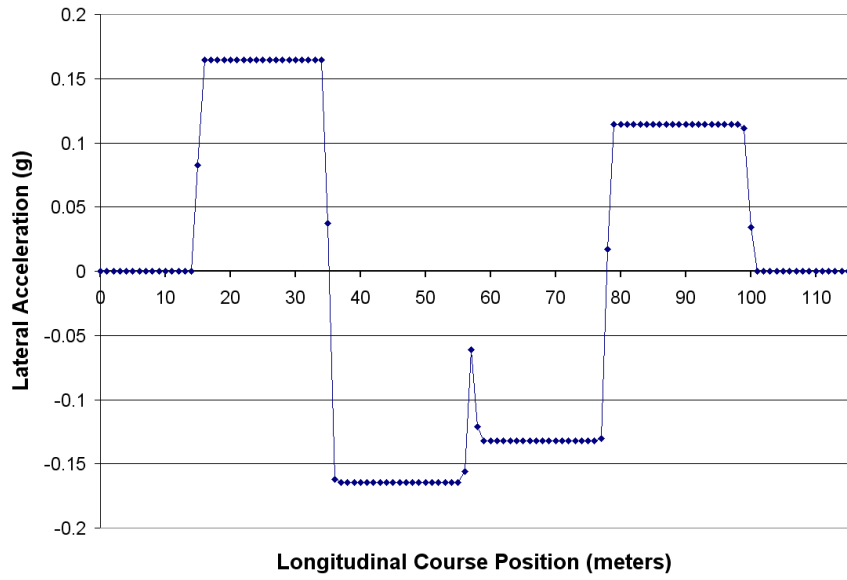
Figure 4.17: 48.3 km/hr (30 mph) Lateral Acceleration Plot
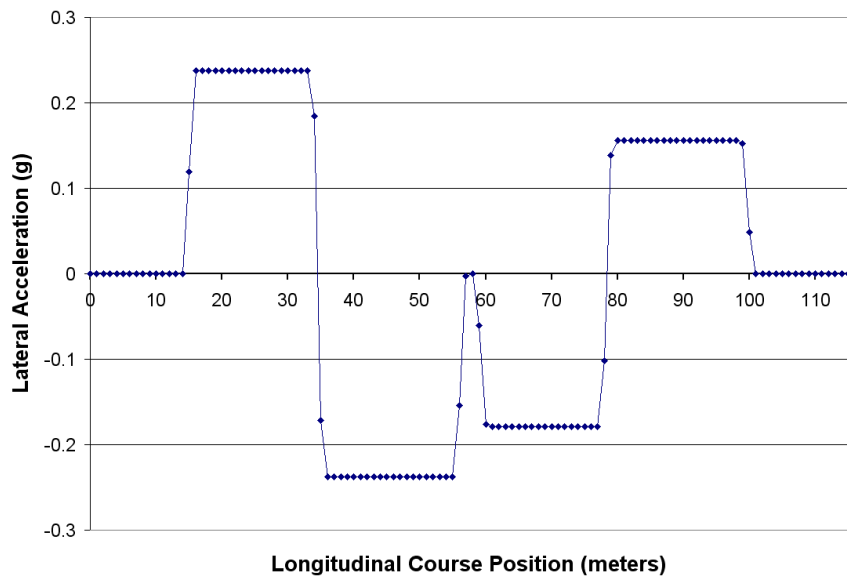
Figure 4.18: 56.3 km/hr (35 mph) Lateral Acceleration Plot
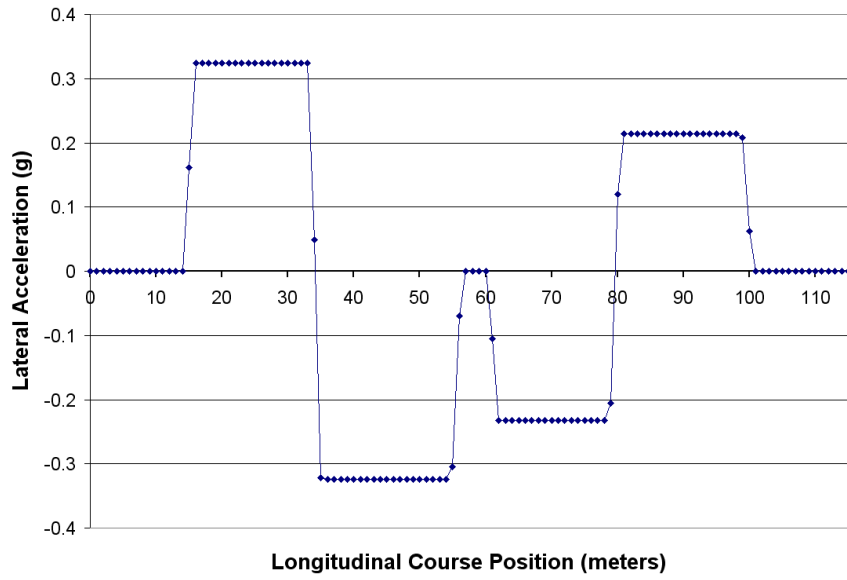
Figure 4.19: 64.4 km/hr (40 mph) Lateral Acceleration Plot
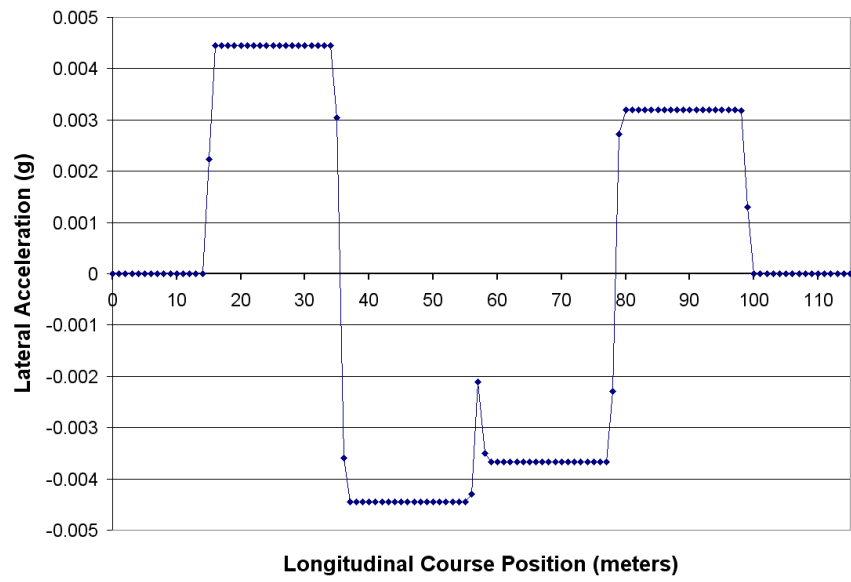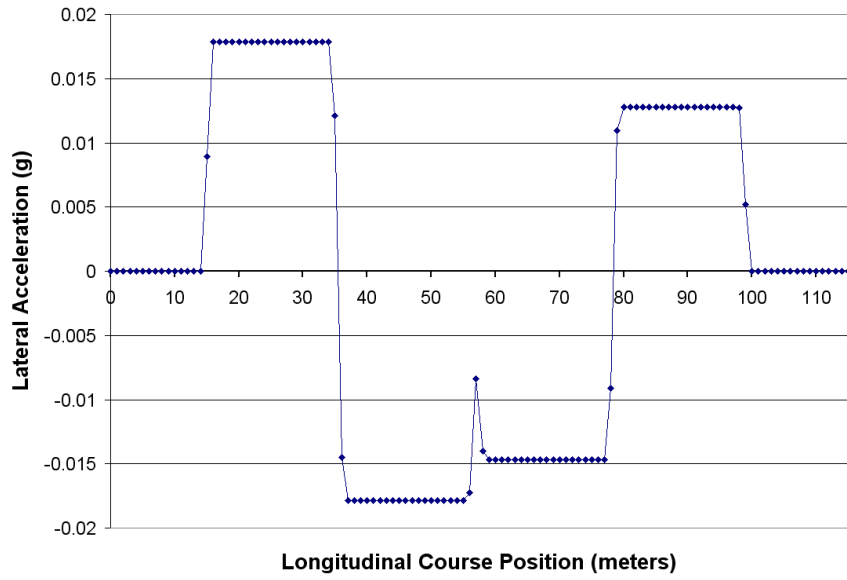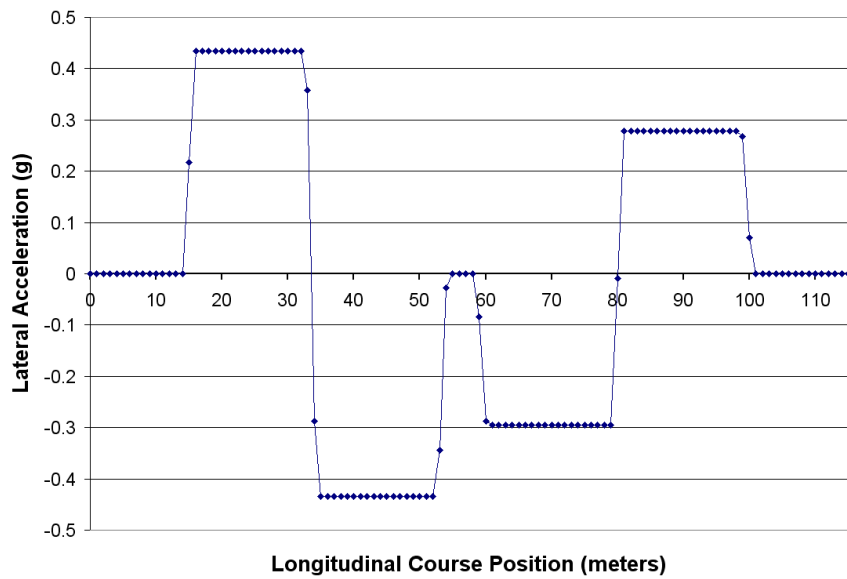

Figure 4.20: 72.4 km/hr (45 mph) Lateral Acceleration Plot

Table 4.1: Path Turn Radius for Each Curved Segment

	Arc 1 R	Arc 2 R	Arc 3 R	Arc 4 R
0 km/hr (0 mph)	113.62	113.62	138.21	147.45
8 km/hr (5 mph)	114.28	114.28	138.78	159.64
16.1 km/hr (10 mph)	114.17	114.17	138.78	159.59
24.1 km/hr (15 mph)	113.81	113.81	138.85	160.87
32.2 km/hr (20 mph)	113.28	113.28	138.92	161.90
40.2 km/hr (25 mph)	112.56	112.56	138.98	163.14
48.3 km/hr (30 mph)	111.30	111.30	139.02	160.28
56.3 km/hr (35 mph)	104.88	104.88	139.54	160.33
64.4 km/hr (40 mph)	100.57	100.57	140.00	151.77
72.4 km/hr (45 mph)	94.89	94.89	139.57	147.79

Table 4.2: Path Curvature for Each Curved Segment

	Arc 1 ρ	Arc 2 ρ	Arc 3 ρ	Arc 4 ρ
0 km/hr (0 mph)	0.0088012	0.0088012	0.0072352	0.0067821
8 km/hr (5 mph)	0.0087503	0.0087503	0.0072055	0.0062639
16.1 km/hr (10 mph)	0.0087586	0.0087586	0.0072055	0.0062659
24.1 km/hr (15 mph)	0.0087867	0.0087867	0.0072019	0.0062162
32.2 km/hr (20 mph)	0.0088274	0.0088274	0.0071986	0.0061765
40.2 km/hr (25 mph)	0.0088839	0.0088839	0.0071951	0.0061298
48.3 km/hr (30 mph)	0.0089850	0.0089850	0.0071931	0.0062392
56.3 km/hr (35 mph)	0.0095346	0.0095346	0.0071665	0.0062371
64.4 km/hr (40 mph)	0.0099430	0.0099430	0.0071430	0.0065890
72.4 km/hr (45 mph)	0.0105389	0.0105389	0.0071648	0.0067662

Table 4.3: Lateral Acceleration Values for Each Curved Segment

	Arc 1 a_y	Arc 2 a_y	Arc 3 a_y	Arc 4 a_y
0 km/hr (0 mph)	0	0	0	0
8 km/hr (5 mph)	0.045	-0.045	-0.004	0.003
16.1 km/hr (10 mph)	0.018	-0.018	-0.015	0.013
24.1 km/hr (15 mph)	0.040	-0.040	-0.033	0.028
32.2 km/hr (20 mph)	0.072	-0.072	-0.059	0.050
40.2 km/hr (25 mph)	0.113	-0.113	-0.092	0.078
48.3 km/hr (30 mph)	0.165	-0.165	-0.132	0.114
56.3 km/hr (35 mph)	0.238	-0.238	-0.179	0.156
64.4 km/hr (40 mph)	0.324	-0.324	-0.233	0.215
72.4 km/hr (45 mph)	0.435	-0.435	-0.295	0.279

Table 4.4: Line Segment Lengths Between Each Arc in Meters

	$d_{1,2}$	$d_{2,3}$	$d_{3,4}$
0 km/hr (0 mph)	0	0.509	0
8 km/hr (5 mph)	0	0.566	0
16.1 km/hr (10 mph)	0	0.570	0
24.1 km/hr (15 mph)	0	0.682	0
32.2 km/hr (20 mph)	0	0.832	0
40.2 km/hr (25 mph)	0	1.037	0
48.3 km/hr (30 mph)	0	0.728	0
56.3 km/hr (35 mph)	0	3.016	0
64.4 km/hr (40 mph)	0	5.395	0
72.4 km/hr (45 mph)	0	5.887	0

$d_{i,j}$ = Length of the line segment between arcs i and j
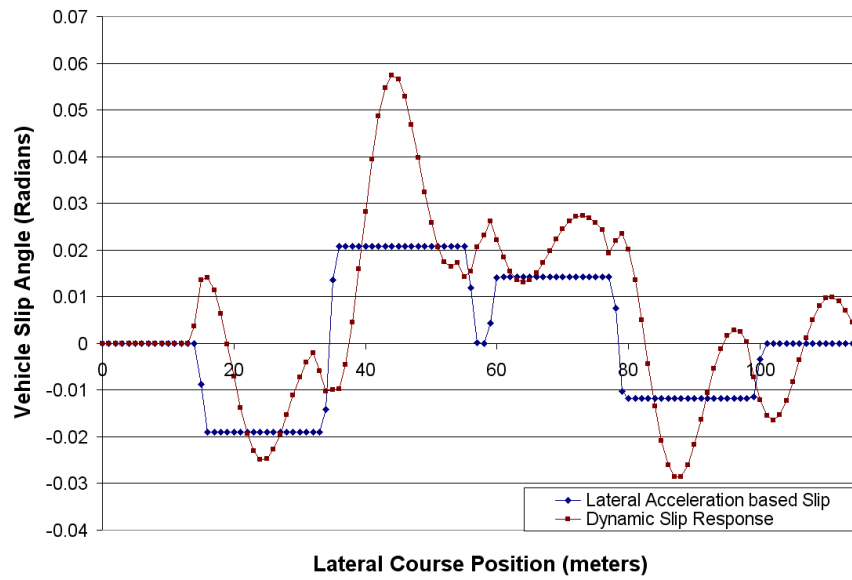
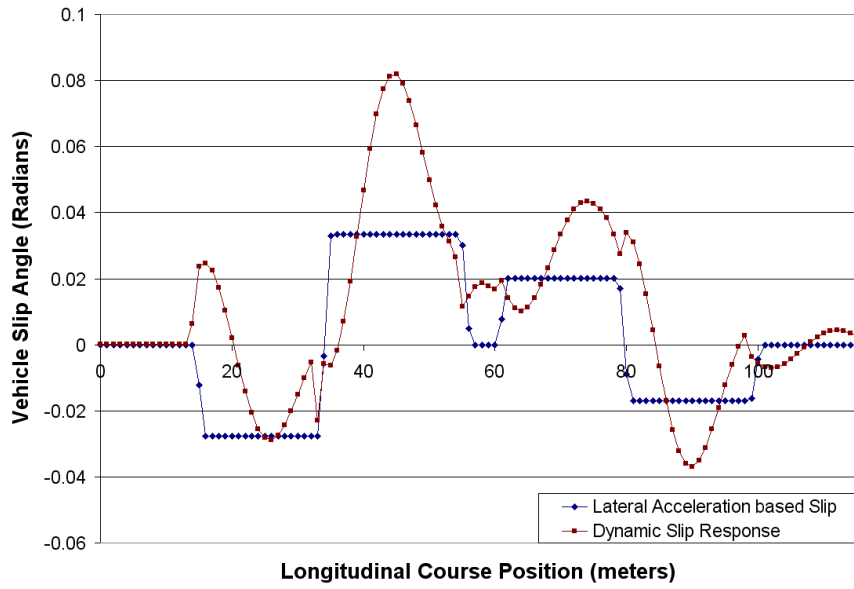Figure 4.21: 56.3 km/hr (35 mph) Vehicle Side-Slip

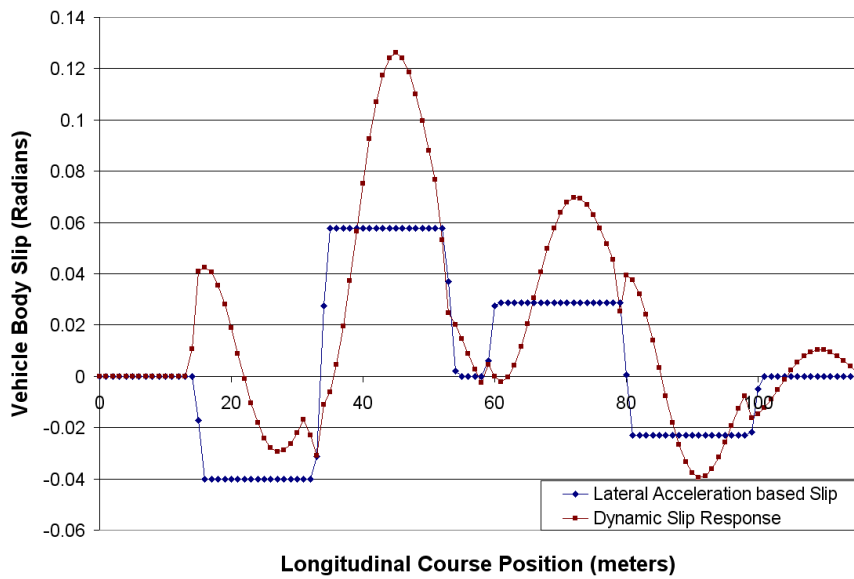Figure 4.22: 64.4 km/hr (40 mph) Vehicle Side-Slip

Figure 4.23: 72.4 km/hr (45 mph) Vehicle Side-Slip

72

4.2   Comparison to Field Data

The optimized speed-dependent model results were compared to field test results from a comparable vehicle. The modelled and field test vehicles had slightly different payload configurations (i.e. slightly different cg and inertia tensor), but were the same vehicle versions with equivalent suspensions and tires. The payload differences were not considered significant enough to invalidate the comparison. Comparing the model output results to current test data provided a validation of the need and usefulness of the model created in this research.

For brevity, only one test speed is compared here. However, the comparison is done at 72.4 km/hr (45 mph), which is very close to the top speed from the field tests. As such, it also presents the most dynamic responses of the vehicle and should have been the hardest conditions for the model to describe.

Figure 4.24 shows a field test path created at 72.4 km/hr (45 mph) with the vehicle's cg trace line in red. This path is compared to a vehicle cg trace generated by the optimization model from Figure 4.9. The corners of the optimization model are omitted to preserve the clarity of the plot. The two paths are very similar, with two small differences. First, the model's path holds a relatively tighter curve after Section 3 of the course. The field test path is relaxed in this region, forcing a tighter turn into Section 5 of the field test. This difference is probably due to driver fear and discomfort. By relaxing the turn out of Section 3, the driver is able to briefly lessen the vehicle's body roll at the cost of increasing the vehicle's dynamic response in the final portion of the test.

The second difference is the angle at which the vehicle enters the test course. Often, field testing does not completely follow the NATO requirement of maintaining a straight and parallel vehicle path in Section 1 (Figure 1.2) of the DLC
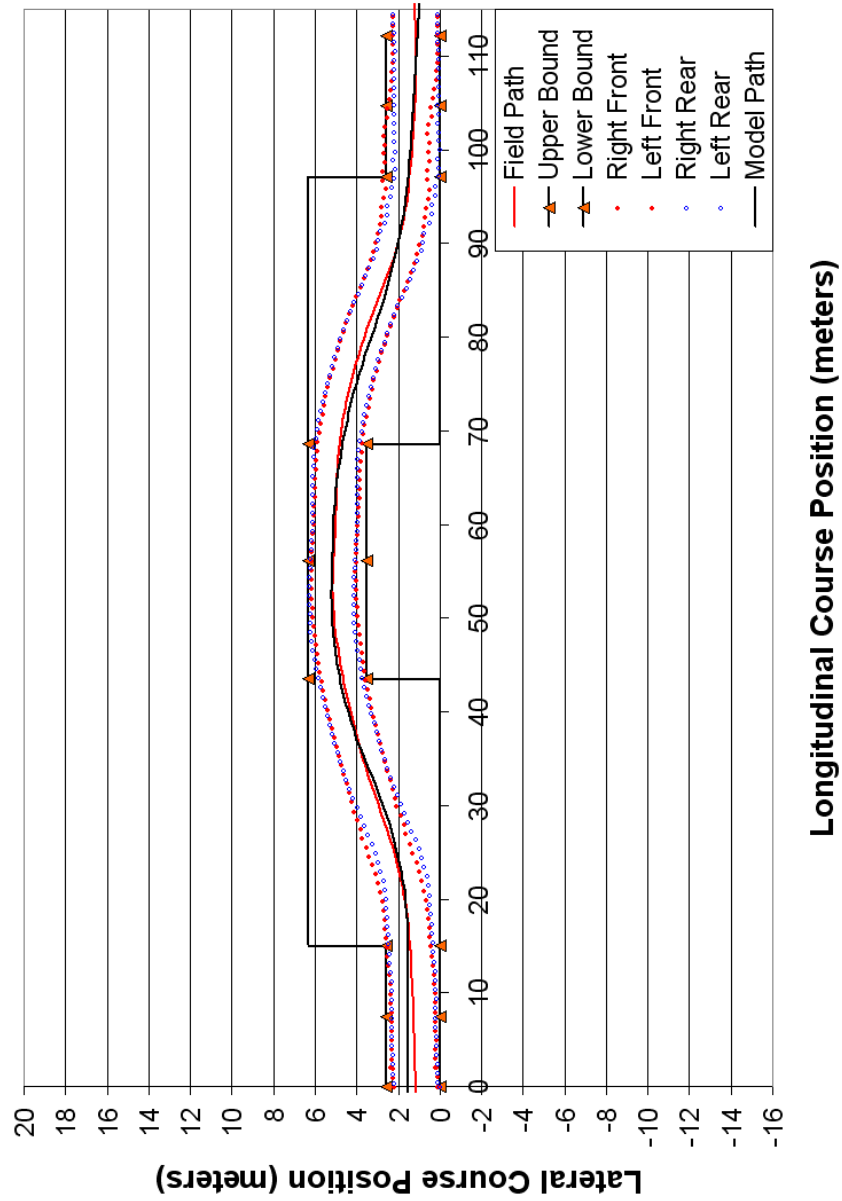
Figure 4.24: 72.4 km/hr (45 mph) Comparison of Field Path Data to Model Path
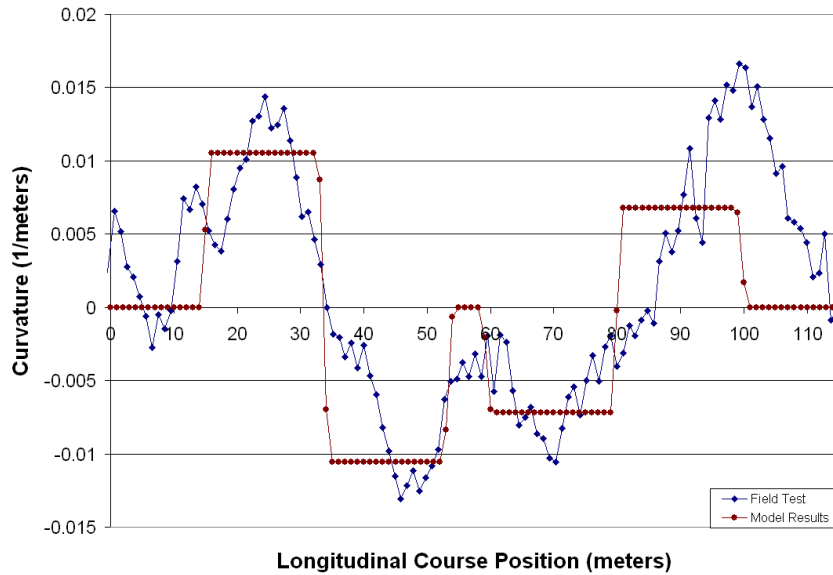
Figure 4.25: 72.4 km/hr (45 mph) Comparison of Field Curvature Data to Model Curvature

maneuver. At the vehicle's limit speed, usually over 64.4 km/hr (40 mph), it is difficult to appropriately follow this testing requirement, because the driver tends to look-ahead and drive accordingly. As a result, drivers tend to enter the test course at various angle. Additionally, drivers begin the first turn prematurely.

The slanted entry angle, and premature turning in Section 1 enable the lateral acceleration values in the first two turns to be reduced. This is shown clearly in Figures 4.25 and 4.26, which plot the path curvature and lateral acceleration values, respectively. If this were not the case, the model's path would display a clear improvement over the test data in the first two turns as it does in the second two. Ultimately, the vehicle optimization model does improve the field test path by minimizing the maximum lateral acceleration from $a_y = 0.66$ to $a_y = 0.43$ gs.
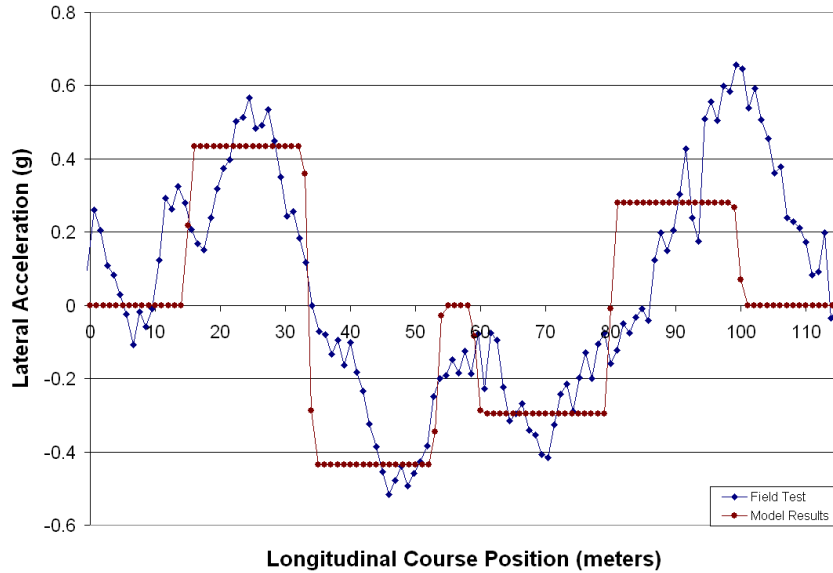
Figure 4.26: 72.4 km/hr (45 mph) Comparison of Field a_y Data to Model a_y

4.3 Comparison to RWS Data

The current testing methods at the RWS are iterative in nature. The DLC test is conducted by predetermining the steering commands for the vehicle. Using these commands the vehicle is tested at a constant forward velocity until a steering command map is generated that enables the vehicle to maneuver through the course without hitting a cone or developing vehicle tip-up. After a feasible steering command is developed, the vehicle speed is increased and the process starts over with the iterative generation of a new steering command.

This intrinsically creates a blind test. It is very difficult for the test operator to determine how the vehicle will respond to the steering command during the test, except from extensive experience. As with the field test, it is often difficult to maintain the NATO requirement of not turning the vehicle until the end of Section

1. It is not difficult, however, to maintain a straight vehicle heading. In contrast to field testing, the RWS test operator is able to test the vehicle's stability limit without fear. This enables the RWS operator to create relatively difficult steering commands, which a field driver would be less apt to make.

Figure 4.27 illustrates the vehicle cg trace and corner locations for a RWS test conducted at 64.4 km/hr (40 mph). The black cg trace is the 64.4 km/hr (40 mph) model result from Figure 4.8. The blind nature of the test produced a long delay before the vehicle entered the third and fourth turns. The result is higher lateral acceleration values through these final turns. This is illustrated in Figures 4.28 and 4.29, which display the curvature and lateral acceleration comparisons, respectively. Similar to the field testing, the improvement made to the second portion of the test is substantial. Overall, the model was able to minimize the maximum lateral acceleration from $a_y = 0.41$ to $a_y = 0.32$ gs.
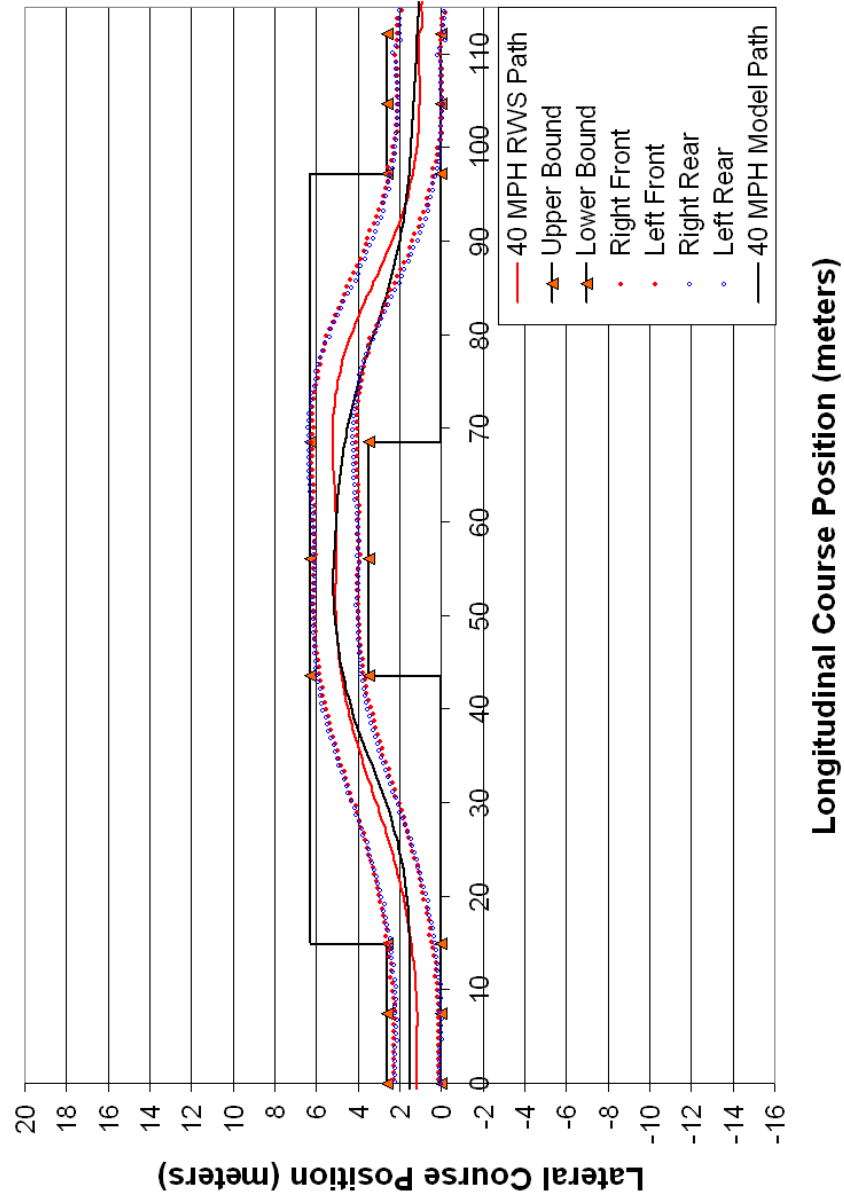
Figure 4.27: 64.4 km/hr (40 mph) Path Comparison of RWS Data to Model Results
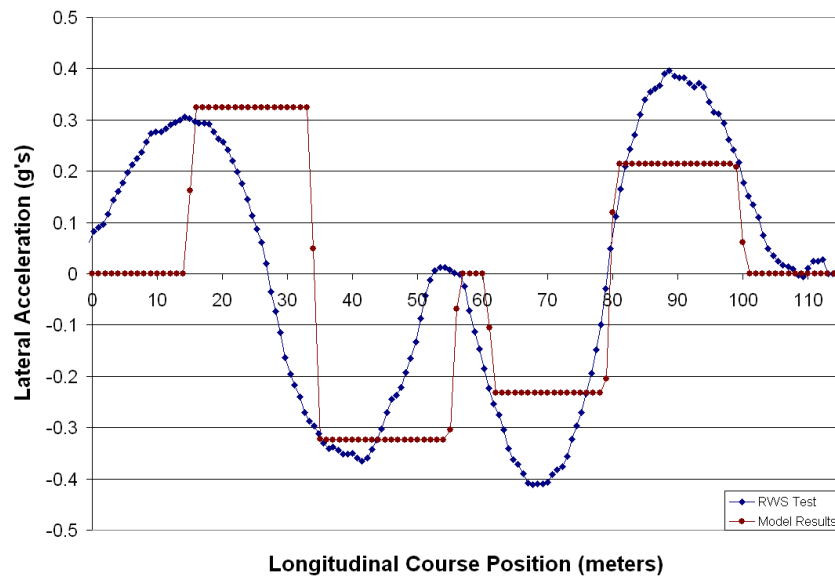
Figure 4.28: 64.4 km/hr (40 mph) Curvature Comparison of RWS Data to Model
Results

4.4 Summary

This chapter demonstrated effective use of the nine-segment vehicle path optimization model at various vehicle speeds. Comparison to field testing and RWS results suggested that this model could improve current testing methods. At progressively higher speeds, increased side-slip did result in differences in the vehicle's path due to the increased dynamics of the vehicle. This result is consistent with field tests where drivers anticipate difficulties later in the course and adjust accordingly.
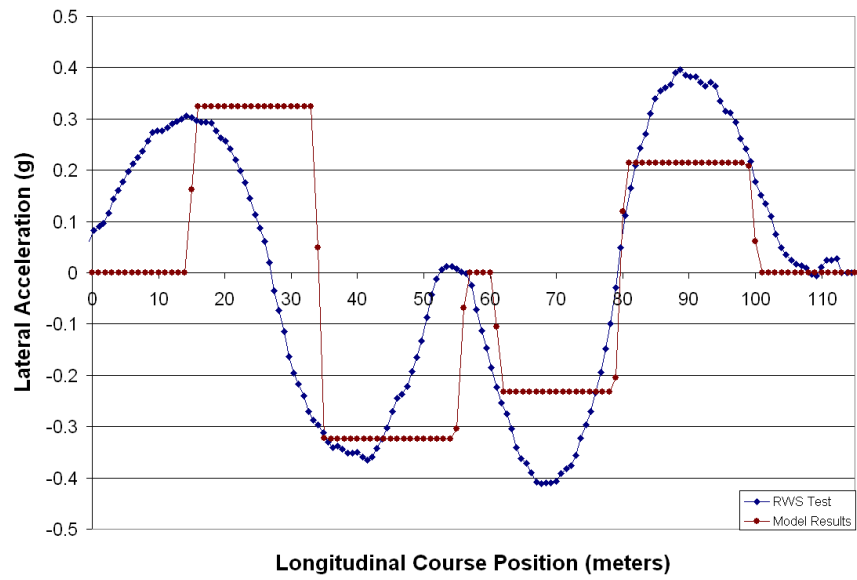
Figure 4.29: 64.4 km/hr (40 mph) a_y Comparison of RWS Data to Model Results

Chapter 5

Conclusions

The research presented in this thesis effectively generated a vehicle path optimization model for vehicle stability testing. The repeatability and adaptability of this vehicle model enabled it to be implemented in simulation tests on the RWS and in field testing. The model will aid in providing an objective test for vehicle stability response. The principles of this research can also be expanded to alternative test course configurations. It is necessary to stress that the objective of the optimization model presented in this paper was to reduce the vehicle's dynamics given a constant test speed and known course constraints.

Path optimization, based on minimization of lateral acceleration, led to the hypothesis that the curve with minimum peak lateral acceleration would be composed of segments of constant curvature. The six-segment and nine-segment models provided further verification that a path composed of constant curvature segments effectively minimized the overall maximum curvature. Further implementation of the nine-segment model demonstrated that the two straight segments between arc one and arc two, and arc three and arc four were unnecessary. This result was intuitive since the elimination of these segments increased the space available to the curved segments. This increased distance provided a larger area over which

the vehicle could change direction, and enabled the localized curvature of the path to further decrease.

The nine-segment model provided significant improvement over initial model construction. The reduced number of primary variables improved the solver's ability to converge toward an effective and optimal path solution. The added constraint of requiring a path to be composed of segments of constant curvature improved the model's ability to approximate an optimal path. Though the solution convergence was improved, the path optimization model is still considered sensitive to large configuration changes. Ensuring convergence necessitates gradual modifications when changes to the model are required, incrementally solving toward the desired path result.

Differences in the curvature values of the four curved segments provided evidence that the constraints of the test course could be altered in the second half of the path to produce more rigorous demands on the end of the vehicle path. Instead, the result was that the path solution was not unique. However, as long as the path variation was beneath the maximum curvature value, the vehicle's stability response generated by the path should remain the same.

It was also discovered that the constant curvature segments produced step response conditions on the vehicle. The lateral acceleration values increased by a square of the vehicle's forward velocity. This step response produced little effect during low speed testing, but becomes important in tests above 48.3 km/hr (30 mph). This required the use of a dynamic side-slip model to determine the vehicle's appropriate slip response to the step forcing conditions. The dynamic transfer function was found to produce an accurate representation of slip response by Kefauver, [16].

82

5.1 Future Work

The hypothesis that an optimal path would consist of constant curvature arcs is yet to be fully proved mathematically. An attempt was made using the principles of optimality and dynamic programming, but a conclusive proof was not obtained. Nonetheless, the basic result was demonstrated with the optimization model produced from this research.

Implementation on the ATC RWS would provide the complete realization of the work presented in this thesis. This would require the generation of a transfer function for generating the vehicle steering commands required to maneuver a given vehicle path. As mentioned earlier, it may be necessary to restrict the vehicle path model using the cushion space provided within the model. This would improve the ability of implementation by providing room for error in the vehicle dynamics used in the vehicle path model.

Real-time implementation on the RWS would also require the use of control techniques, such as feed-forward. Follow the carrot, and other control techniques that use a look ahead distance may provide further insight into the real-time path control needed for appropriate implementation.

An additional area of interest is the effect of the step response caused by the transition between the segments of constant curvature arcs. An interesting investigation would compare test results of constant curvature paths to paths with a limited rate of change of curvature in addition to limited path curvature. However, it would be difficult to determine appropriate limitations for the rate of change of the path's curvature.

Appendix A

Calculations

A.1   Six Segment Constant Radius Arc Path
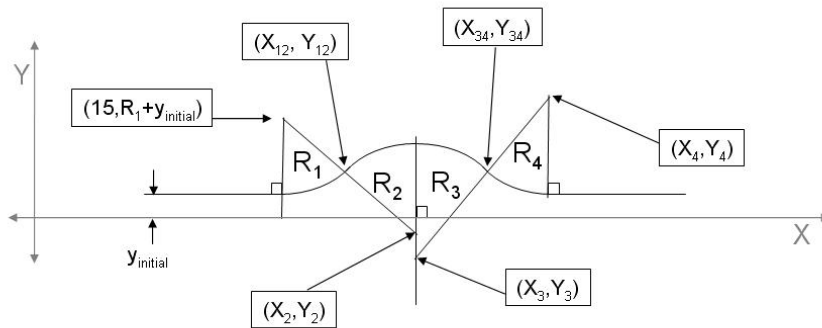

Figure A.1: A Vehicle Path Composed of Six Curve Segments

A.1.1   Definitions

$$R_i \quad = \quad the\ radius\ of\ arc\ i$$

$$(x_{Ri}, y_{Ri}) \quad = \quad coordinates\ of\ the\ center\ point\ for\ the\ constant\ radius\ arc\ i$$

$$(x_{ij}, y_{ij}) = \text{coordinates of transition point between arc } i \text{ and arc } j$$

<div align="right">(A.1)</div>

A.1.2   Variables

$$y_{initial} = \text{lateral distance from the longitudinal axis for Section 1}$$

$$R_1 = \text{Radius of the first arc}$$

$$R_3 = \text{Radius of the third arc}$$

$$x_{12} = \text{x value of the inflection point between arc 1 and 2}$$

$$x_{R2} = \text{x value of center point of arc 2}$$

$$x_{34} = \text{x value of the inflection point between arc 3 and 4}$$

$$x_{R4} = \text{x value of center point of arc 4}$$

A.1.3   Spreadsheet Relationships

$$R_2 = \sqrt{(x_{12} - x_{R2})^2 + (y_{12} - y_{R2})^2} \tag{A.2}$$

$$R_4 = \sqrt{(x_{34} - x_{R4})^2 + (y_{34} - y_{R4})^2} \tag{A.3}$$

$$y_{R1} = R_1 + y_{initial} \tag{A.4}$$

$$y_{12} = R_1 + y_{initial} - \sqrt{R_1^2 - x_{12}^2 + 30x_{12} - 225} \tag{A.5}$$

$$y_{R2} = y_{R1} - (x_{R1} - x_{R2})\frac{(y_{R1} - y_{12})}{(x_{R1} - x_{12})} \tag{A.6}$$

$$x_{R3} = x_{R2} \tag{A.7}$$

$$y_{R3} = y_{R2} + R_2 - R_3 \tag{A.8}$$

$$y_{34} = y_{R3} + \sqrt{2x_{R3}x_{34} + R_3^2 - x_{34}^2 - x_{R3}^2} \tag{A.9}$$

$$y_{R4} = y_{R3} - (x_{R3} - x_{R4})\frac{(y_{R3} - y_{34})}{(x_{R3} - x_{34})} \tag{A.10}$$

$$\text{(A.11)}$$

A.1.4 Lateral Position Equation for each segment given x_i

$$
\begin{aligned}
y_1 &= y_{initial} & \text{(A.12)} \\
y_2 &= R_1 + y_{initial} - \sqrt{R_1^2 - x_i^2 + 30x_i - 225} & \text{(A.13)} \\
y_3 &= y_{R2} + \sqrt{2x_{R2}x_i + R_2^2 - x_i^2 - x_{R2}^2} & \text{(A.14)} \\
y_4 &= y_{R3} + \sqrt{2x_{R3}x_i + R_3^2 - x_i^2 - x_{R3}^2} & \text{(A.15)} \\
y_5 &= y_{R4} - \sqrt{2x_{R4}x_i + R_4^2 - x_i^2 - x_{R4}^2} & \text{(A.16)} \\
y_6 &= y_{R4} - R_4^2 & \text{(A.17)} \\
& & \text{(A.18)}
\end{aligned}
$$

A.2 Nine Segment Constant Radius Arc Path
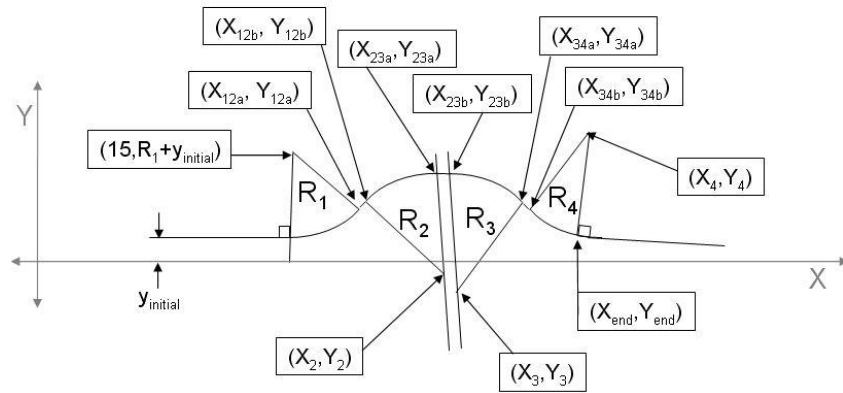
Figure A.2: A Vehicle Path Composed of Nine Curve Segments

A.2.1 Definitions

$$
\begin{aligned}
R_i &= \textit{the radius of arc } i \\
(x_{Ri}, y_{Ri}) &= \textit{coordinates of the center point for the constant radius arc } i \\
\textit{line } ij &= \textit{the straight segment line between arc } i \textit{ and arc } j \\
(x_{ija}, y_{ija}) &= \textit{coordinates of the transition point between arc } i \textit{ and line } ij \\
(x_{ijb}, y_{ijb}) &= \textit{coordinates of the transition point between line } ij \textit{ and arc } j \\
m_{ij} &= \textit{slope of the line normal to line } ij \\
d_{ij} &= \textit{length of the line } ij
\end{aligned}
$$

A.2.2 Variables

$$
\begin{aligned}
y_{initial} &= \textit{lateral distance from the longitudinal axis for Section 1} \\
R_1 &= \textit{Radius of the first arc} \\
R_3 &= \textit{Radius of the third arc} \\
x_{12a} &= \textit{x value of the intersection point between arc 1 and line 12} \\
x_{12b} &= \textit{x value of the intersection point between line 12 and arc 2} \\
x_{R2} &= \textit{x value of center point of arc 2} \\
x_{23a} &= \textit{x value of the intersection point between arc 2 and line 23} \\
x_{23b} &= \textit{x value of the intersection point between line 23 and arc 3} \\
x_{34a} &= \textit{x value of the intersection point between arc 3 and line 34} \\
x_{34b} &= \textit{x value of the intersection point between line 34 and arc 4} \\
x_{R4} &= \textit{x value of center point of arc 4} \\
x_{end} &= \textit{End of fourth arc and beginning of final straight section}
\end{aligned}
$$

A.2.3 Spreadsheet Relationships

$$R_2 = \sqrt{(x_{12b} - x_{R2})^2 + (y_{12b} - y_{R2})^2} \tag{A.19}$$

$$R_4 = \sqrt{(x_{34b} - x_{R4})^2 + (y_{34b} - y_{R4})^2} \tag{A.20}$$

$$y_{R1} = R_1 + y_{initial} \tag{A.21}$$

$$y_{12a} = y_{R1} - \sqrt{R_1^2 - x_{12a}^2 + 30x_{12a} - 225} \tag{A.22}$$

$$\frac{1}{m_{12}} = \frac{x_{12a} - x_{R1}}{y_{12a} - y_{R1}} \tag{A.23}$$

$$d_{12} = \sqrt{(x_{12b} - x_{12a})^2 + (y_{12b} - y_{12a})^2} \tag{A.24}$$

$$y_{12b} = y_{12a} + \frac{1}{m_{12}}(x_{12a} - x_{12b}) \tag{A.25}$$

$$y_{R2} = m_{12}(x_{R2} - x_{12b}) + y_{12b} \tag{A.26}$$

$$y_{23a} = y_{R2} + \sqrt{R_2^2 - (x_{R2} - x_{23a})^2} \tag{A.27}$$

$$\frac{1}{m_{23}} = \frac{x_{23a} - x_{R2}}{y_{23a} - y_{R2}} \tag{A.28}$$

$$d_{23} = \sqrt{(x_{23b} - x_{23a})^2 + (y_{23b} - y_{23a})^2} \tag{A.29}$$

$$y_{23b} = y_{23a} + \frac{1}{m_{23}}(x_{23a} - x_{23b}) \tag{A.30}$$

$$x_{R3} = x_{23b} - \frac{1}{m_{23}}(y_{23b} - y_{R3}) \tag{A.31}$$

$$y_{R3} = y_{R2} + R_2 - R_3 \tag{A.32}$$

$$y_{34a} = y_{R3} + \sqrt{2x_{R3}x_{34a} + R_3^2 - x_{34a}^2 - x_{R3}^2} \tag{A.33}$$

$$\frac{1}{m_{34}} = \frac{x_{34a} - x_{R3}}{y_{34a} - y_{R3}} \tag{A.34}$$

$$d_{34} = \sqrt{(x_{34b} - x_{34a})^2 + (y_{34b} - y_{34a})^2} \tag{A.35}$$

$$y_{34b} = y_{34a} + \frac{1}{m_{34}}(x_{34a} - x_{34b}) \tag{A.36}$$

$$y_{R4} = y_{R3} - (x_{R3} - x_{R4})\frac{(y_{R3} - y_{34b})}{(x_{R3} - x_{34b})} \tag{A.37}$$

A.2.4 Lateral Position Equation for each segment given x_i

$$y_1 = y_{initial} \tag{A.38}$$

$$y_2 = R_1 + y_{initial} - \sqrt{R_1^2 - x_i^2 + 30x_i - 225} \tag{A.39}$$

$$y_3 = y_{12a} + \frac{1}{m_{12}}(x_{12a} - x_i) \tag{A.40}$$

$$y_4 = y_{R2} + \sqrt{2x_{R2}x_i + R_2^2 - x_i^2 - x_{R2}^2} \tag{A.41}$$

$$y_5 = y_{23a} + \frac{1}{m_{23}}(x_{23a} - x_i) \tag{A.42}$$

$$y_6 = y_{R3} + \sqrt{2x_{R3}x_i + R_3^2 - x_i^2 - x_{R3}^2} \tag{A.43}$$

$$y_7 = y_{34a} + \frac{1}{m_{34}}(x_{34a} - x_i) \tag{A.44}$$

$$y_8 = y_{R4} - \sqrt{2x_{R4}x_i + R_4^2 - x_i^2 - x_{R4}^2} \tag{A.45}$$

$$y_9 = y_{end} + \frac{1}{m_{end}}(x_{end} - x_i) \tag{A.46}$$

BIBLIOGRAPHY

[1] Allen, R.W., Christos, J.P., etc., 2002, "Driver/Vehicle Modeling and Simulation", SAE Transations Paper No. 2002-01-1568.

[2] Allen, R.W., Rosenthal, T.J., etc., 1999, "Computer Simulation Analysis of Light Vehicle Lateral/Directional Dynamic Stability", SAE Transactions Paper No. 1999-01-0124.

[3] Bernard, J., Gruening, J., and Hoffmeister, K., 1998, "Evaluation of Vehicle/Driver Performance Using Genetic Algoritms", SAE Transactions Paper No. 980227.

[4] U.S. Department of Transportation NHTSA: *Traffic Safety Facts 2002*. Washington DC 2004.

[5] Flystra, D., Lasdon, L., Watson, J. and Waren, A., 1998, "Design and Use of the Microsoft Excel Solver", *Interfaces*, **28**, No. 5, pp. 29-55.

[6] Fraichard, T., and Scheuer, A., 2004, "From Reeds and Shepp's to Continuous-Curvature Paths", *IEEE Transactions on Robotics*, **20**, NO. 6, pp. 1025-1035.

[7] Forkenbrock, G.J., Garrott, W.R., 2002, "Light Vehicle Dynamic Rollover Propensity Phases IV, V, and VI: Research Activities", Unpublished NHTSA presentation (http://www-nrd.nhtsa.dot.gov/pdf/nrd-01/SAE/SAE2002/RGarrott_rollover.pdf).

[8] Forkenbrock, G.J., Heitz, M., etc., 2003, "An Experimental Examination of J-Turn and Fishhook Maneuvers That May Induce On-Road, Untripped, Light Vehicle Rollover", SAE Transactions Paper No. 2003-01-1008.

[9] Forkenbrock, G.J., Heitz, M, etc., 2003, "An Experimental Examination of Double Lane Change Maneuvers That May Induce On-Road, Untripped, Light Vehicle Rollover", SAE Transactions Paper No. 2003-01-1009.

[10] Forkenbrock, G.J., O'Harra, B.C., Elsasser D. 2003, "An Experimental Examination of 26 Light Vehicles Using Test Maneuvers That May Induce On-Road, Untripped Rollover and a Discussion of NHTSAs Refined Test Procedures -Phases VI and VII of NHTSAs Light Vehicle Rollover Research Program", U.S. Department of Transportation Report No. DOT HS 809 547.

[11] Frimberger, M., Wolf, F., Scholpp, G. etc., 2000, "Influences of Parameters at Vehicle Rollover", SAE Transactions Paper No. 2000-01-2669.

[12] Gillespie, T.D. 1992, *Fundamentals of Vehicle Dynamics*, Society of Automotive Engineers, Warrendale, PA.

[13] Gruening, J., Bernard, J., Clover, C. etc., 1998, "Driving Simulation", SAE Transactions Paper No. 980223.

[14] Guan, H., Gao, Z., Guo, K. etc., 2000, "A Driver Direction Control Model and its Application in the Simulation of Driver-Vehicle-Road Closed-Loop System", SAE Transactions Paper No. 2000-01-2184.

[15] Guan, H., Gao, Z. and Guo, K., 2000, "Driver Fuzzy Decision Making Model of Vehicle Preview Course", SAE Transactions Paper No. 2000-01-3057.

[16] Kefauver, K., 2005, "Dynamic Side-Slip Transfer Function for Lateral Acceleration Step Response on a Light-Duty Utility Military Tactical Vehicle", U.S. Army Aberdeen Test Center's Roadway Simulator, unpublished notes.

[17] Langer, W., 1995, "Validation of Flat Surface Roadway Technology", Society of Automotive Engineers Paper No. 950310.

[18] Langer, W., 1996, "Vehicle Testing With Flat Surface Roadway Technology", Society of Automotive Engineers Paper No. 960731.

[19] Lasdon, L.S. and Smith, S., 1992, "Solving large sparse nonlinear programs using GRG", ORSA Journal on Computing, Vol. 4, No. 1, pp. 2-15.

[20] Marine, M.C., Wirth, J.L. and Thomas, T.M., 1999, "Characteristics of On-Road Rollovers", SAE Transactions Paper No. 1999-01-0122.

[21] Milliken, W.F., Milliken, D.L., 1995, *Race Car Vehicle Dynamics*, Society of Automotive Engineers, Warrendale, PA.

[22] Naudé, A.F., Steyn, J.L., 1993, "Objective Evaluation of the Simulated Handling Characteristics of a Vehicle in a Double Lane Change Manoeuvre", SAE Transactions Paper No. 930826.

[23] Polhemus, V.D. 1970, "Road Simulator Facility", United States Patent No. 3,520,180

[24] Prokop, G., 2001, "Modeling Human Vehicle Driving by Model Predictive Online Optimization", Vehicle System Dynamics, **35**, No. 1, pp. 19-53.

[25] Renski, A., 1998, "The Driver Model and Identification of Its Parameters", SAE Transactions Paper No. 980011.

[26] Salaani, M.K., Heydinger, G. and Grygier., P., 2002, "Modeling and Implementation of Steering System Feedback for the National Advanced Driving Simulator", SAE Transactions Paper No. 2002-01-1573.

[27] Schultz, G.A., 2003, Undergraduate Vehicle Dynamics course. From unpublished lecture notes.

[28] Schultz, G.A., Tong, I., Kefauver, K. and Ishibashi, J. (2005) 'Steering and Handling Testing Using Roadway Simulator Technology", *Int. J. of Vehicle Systems Modeling and Testing*, To be published.

[29] Tseng, H.E., Asgari, J., Cherry, A., Neads, S., etc., 2004, "Steering Robot for Evasive Maneuvers - Experiment and Analysis", IFAC Conference on Mechatronic Systems, pg. 87-95.

[30] Yan, Q. Williams, J.M., and Li, J. 2002, "Chassis Control System Development Using Simulation: Software in the Loop, Rapid Prototyping and Hardware in the Loop", SAE Transactions Paper No. 2002-01-1565